NUMERICAL AND APPROXIMATE SOLUTIONS TO PROBLEMS IN SPONTANEOUS IGNITION

A thesis presented in partial fulfilment of
the requirements for the degree of
Master of Philosophy
in Mathematics at
Massey University

Catherine Margaret Rivers

1994

ABSTRACT

This thesis considers the subject of time-independent spontaneous ignition of materials of arbitrary shape.

Chapter One reviews the major advances up to the work of D.A.Frank-Kamenetskii.

Chapter Two discusses the modern, Gray Wake, formulation of the problem.

In Chapter Three, ignition in the class A shapes is approximated by a numerical finite differences method. The same method is applied to some non-class A geometries.

Solutions to the Gray Wake formulation for ignition in the infinite slab geometry are sought in Chapter Four by approximating the internal energy gradient by the maximum internal energy and by the average internal energy.

Chapter Five considers an industrial application of the spontaneous ignition of moist powder.

CONTENTS

1 INTRODUCTION

1.1 Background

In 1993, at 3:00 am on Good Friday, an explosion occurred in the milk powder factory at Te Rapa, New Zealand (see Figure 1.1). The fire, whose cause is unexplained, resulted in an explosion of milk powder. Extensive damage was caused. The plant, believed to be the largest in the southern hemisphere, was closed for some months at great cost to the parent company.

When materials which contain a heat source are stored in ambient temperatures at or below their internal temperatures, the generated heat builds up to levels where ignition can occur. Powdery masses, like the milk at Te Rapa, can burst into flame, or can explode. The phenomenon is known as spontaneous ignition.

The behaviour and the control of spontaneous ignition is of interest. How hot can materials be assembled? To what temperature should materials be cooled before being stored? Given assembly and storage conditions, what mass of material can be accumulated safely? Can spontaneous ignition be used as a positive factor in manufacturing processes?

Rules of thumb have been developed in many trades, industries and occupations to diminish the risk of spontaneous ignition in the assembly and storage of materials.

Techniques are required to describe the ignition behaviour of materials and to predict safe working limits within which materials can be handled. Modern researchers have endeavoured to disclose the underlying model for spontaneous ignition. This study is a part of that process.

FIGURE 1.1 The aftermath of a dust expolsion.

1.2 Thermodynamic Basis for Ignition

For the elementary reaction A $\Leftrightarrow$ B, the activation energy is the energy required to allow the reaction to occur. The greater the activation energy, the fewer are the collisions involving sufficient energy to cause reaction at a given temperature, and the slower is the reaction. As the temperature is increased, more collisions comprise energy equal to or greater than the activation energy, and the reaction rate becomes greater.

For small changes in temperature, the dependence of rate constant on temperature can be represented by the Arrhenius equation,

$$k = A\exp(-E/RT) \tag{1.1}$$

where A is the pre-exponential factor, E is the activation energy, R is the Universal Gas Constant and T is the temperature.

Thermal ignition is an exothermic reaction. Neglecting reactant consumption, the heat balance equation is

$$\nabla\cdot(\kappa\nabla T) + \sigma QA\exp(-E/RT) = C\frac{\partial T}{\partial t} \tag{1.2}$$

where κ is the thermal conductivity, T the temperature, σ is the density, Q is the exothermicity, C is the heat capacity and t represents time.

The Biot number is the ratio of surface heat transfer to thermal conductivity. If Bi$\rightarrow$0, the temperature becomes uniform throughout the region and there is an abrupt temperature drop at the interface with the surroundings down to the ambient temperature. If Bi$\rightarrow\infty$, the temperature at the boundary becomes equal to the ambient temperature; that is, the boundary condition is

$$T = T_a \tag{1.3}$$

and a temperature gradient exists within the reaction zone. The zero Biot number scenario was developed by Semenov and others; the infinite Biot number by Frank-Kamenetskii and others.

1.3 Frank-Kamenetskii Conditions

In the steady-state equation, $\partial T / \partial t = 0$. For the class A geometries of infinite slab, infinite cylinder and sphere, the steady-state formulation has been investigated by Frank-Kamenetskii as

$$\begin{aligned} \nabla^2\theta + \delta\exp\left(\frac{\theta}{1+\varepsilon\theta}\right) = 0 \qquad & \text{in the region with} \\ \theta = 0 \qquad & \text{on the boundary} \end{aligned} \tag{1.4}$$

with the dimensionless energy parameter,

$$\varepsilon = \frac{RT_a}{E}, \tag{1.5}$$

and the dimensionless Frank-Kamenetskii eigenvalue parameter,

$$\delta = \frac{\sigma Q a_0^2 EA \exp(-E/RT_a)}{\kappa RT_a^2}, \tag{1.6}$$

for which a_0 is some characteristic half-width of the region containing the reaction.

The variable θ represents the dimensionless temperature rise above ambient temperature,

$$\begin{aligned} \theta &= \frac{1}{\varepsilon}\cdot\frac{T-T_a}{T_a} \\ &= \frac{E}{RT_a^2}(T-T_a). \end{aligned} \tag{1.7}$$

The effect on the solution θ of varying δ while keeping ε fixed is shown in Figure 1.3. Of interest is δ_{cr}, the value of δ at which the first bifurcation point occurs on the minimal branch. If $\delta < \delta_{cr}$, the material will warm and will reach a steady temperature distribution; if $\delta > \delta_{cr}$, the material will eventually heat to the point of ignition, that is, thermal runaway may occur; if $\delta = \delta_{cr}$, a metastable state exists.

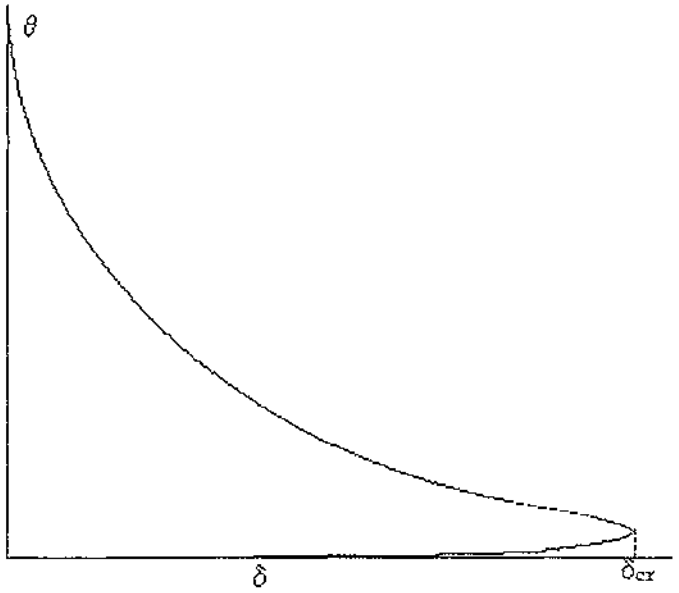

FIGURE 1.2 Bifurcation diagram.

When $\varepsilon << 1$, the instantaneous heat balance equation can be written as

$$\begin{aligned} \frac{d^2\theta}{d\rho^2} + \frac{j}{\rho}\frac{d\theta}{d\rho} + \delta\exp(\theta) &= 0 \\ \theta\big|_{\rho=1} &= 0 \\ \left.\frac{d\theta}{d\rho}\right|_{\rho=0} &= 0 \end{aligned} \tag{1.8}$$

where the dimensionless shape factor, j, has value 0 for slab, 1 for cylinder and 2 for sphere. The variable ρ is a function of distance, r, from the centre of the body;

$$\rho = \frac{r}{a_0}. \tag{1.9}$$

In general, the boundary condition is

$$\begin{aligned} \frac{ha_0}{\kappa}\theta_s &= \begin{cases} \mp\dfrac{d\theta}{d\rho} & \text{when } j = 0, \text{ i.e. when } \rho = \pm 1 \\ -\dfrac{d\theta}{d\rho} & \text{when } j = 1,2, \text{ i.e. when } \rho = 1,2 \end{cases} \\ &= Bi\,\theta_s \end{aligned} \tag{1.10}$$

where h is the surface heat transfer coefficient and θ_s is the dimensionless temperature excess at the surface.

By symmetry,

$$\frac{d\theta}{d\rho} = 0 \qquad \text{when } \rho=0. \tag{1.11}$$

Equation (1.4) cannot be solved explicitly when ε is non-zero. Solution of (1.8) yields the values in Table 1.1.

Shape	δ_{cr}	
infinite slab	0.88	(analytical)
infinite cylinder	2.00	(analytical)
sphere	3.32	(no exact solution)

TABLE 1.1

The variation of δ_{cr} with Bi is shown in Figure 1.3. Under Semenov conditions (Bi→0), Bi and δ_{cr} are related by

$$\delta_{cr} = (j+1)\frac{Bi}{e} \tag{1.12}$$

shown in Figure 1.3 by the dashed line. When Bi is small, δ_{cr} is proportional to Bi. As Bi becomes larger, δ_{cr} tends asymptotically to a maximum value, the Frank-Kamenetskii limit.

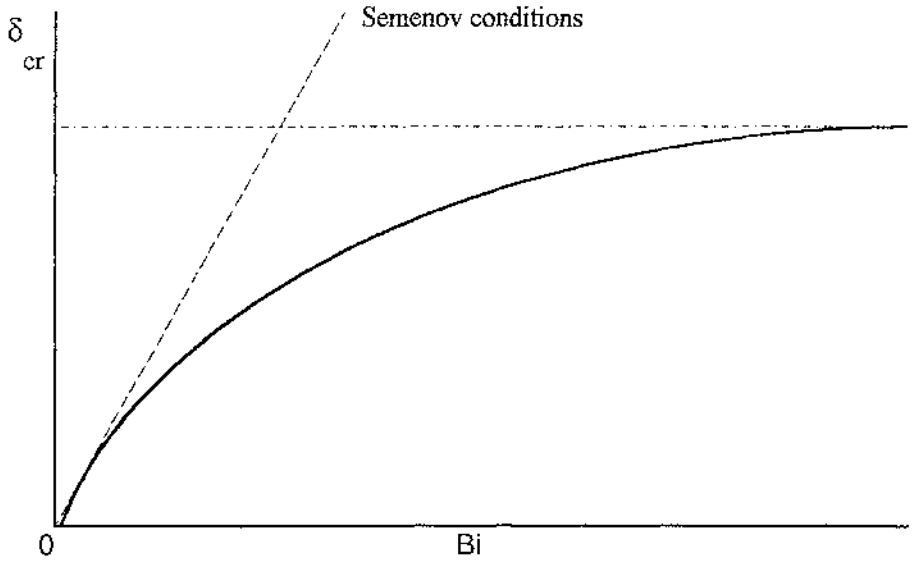

FIGURE 1.3 Variation of δ_{cr} with Biot number, Bi.

2 MODERN FORMULATION

In practice, δ_{cr} and Bi are not as useful as critical ambient temperature, critical initial temperature and critical size in determining the conditions for spontaneous ignition. The latter are easier to determine *in situ* and are of more practical interest than δ_{cr} or Bi in the causal determination and prevention of fires.

When

$$u = \frac{RT}{E}$$
$$U = \frac{RT_a}{E} \tag{2.1}$$

the steady state formulation for combustion in the slab geometry, Equation (1.4), can be written as

$$\nabla^2 u + \lambda \exp\left(-\frac{1}{u}\right) = 0 \qquad \text{in the region } \Omega \tag{2.2}$$

with

$$\frac{\partial u}{\partial n} + \mathrm{Bi}(u - U) = 0 \qquad \text{on the boundary } \partial\Omega$$

where

$$\lambda = \frac{\sigma Q A R a_0^2}{\kappa E} \tag{2.3}$$

and $\partial u / \partial n$ is the outward normal derivative at the boundary.

The ambient temperature, T_a, becomes the natural control parameter since it is easily monitored in a practical situation and appears only in U, in contrast to the Frank-Kamenetskii formulation in which T_a appears in θ, δ and ε. The distinguished parameter is U. Thus, the critical ambient temperature can be read directly from a graph of u v. U via (2.1).

Another benefit of the modern formulation is that the Frank-Kamenetskii length variable, a_0, appears only in the expression for λ. The dimensionless variables and parameters, u_1, u_a and λ, are known as the Gray Wake variables and parameters. The transformation is

$$u_a = \varepsilon$$
$$\lambda = \delta e^{\frac{1}{\varepsilon}} \varepsilon^2. \tag{2.4}$$

The bifurcation diagram for fixed value of λ is shown in Figure 2.1. Stable and unstable branches are indicated by labels *s* and *u* respectively.

The point of ignition corresponds to the first fold bifurcation point, occurring at U_{cr}, the critical value of U. For values of U slightly greater than U_{cr}, the system migrates to the upper stable branch involving much greater internal energy, *u*; ignition thus occurs.

When a fire already exists, the internal energy is high and the system corresponds to a point on the upper stable branch. As the internal energy is reduced, the system reaches the second fold bifurcation point. A slight decrease in energy causes the system to fall to the lower stable branch involving much lower internal energy, *u*; extinction thus occurs.

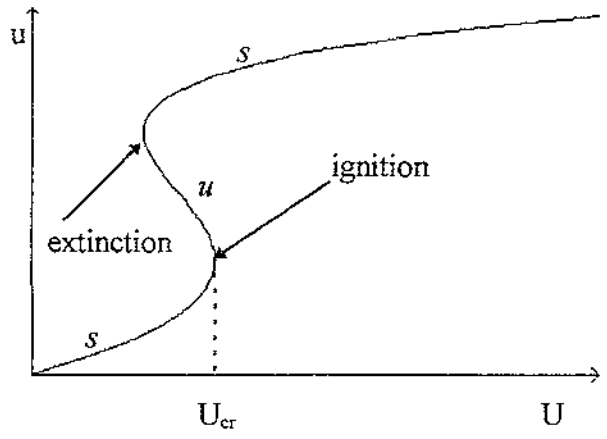

FIGURE 2.1 Bifurcation diagram for the infinite slab.

Gray and Wake [14] have shown that non-trivial solutions to the heat balance equation exist when U=0 for large λ. That is, an upper stable branch exists, even when the bifurcation curve is discontinuous.

The uniform reaction has equation

$$u - U = \lambda \exp\left(-\frac{1}{u}\right) \tag{2.5}$$

The bifurcation diagram is shown in Figure 2.2.

There is always a unique solution for small λ. As λ increases, the curve adopts more of an s-shape until multiplicity first occurs at $\lambda = \lambda_{tr}$. For values of λ greater than λ_{tr}, the minimal branch becomes discontinuous at $\lambda = \lambda_{cr}$. Multiplicity first occurs for the absolute zero case (U=0) at $\lambda = \lambda'$. Burnell *et al* [8] have shown that, for the slab geometry, $\lambda_{tr} = 4.618$.

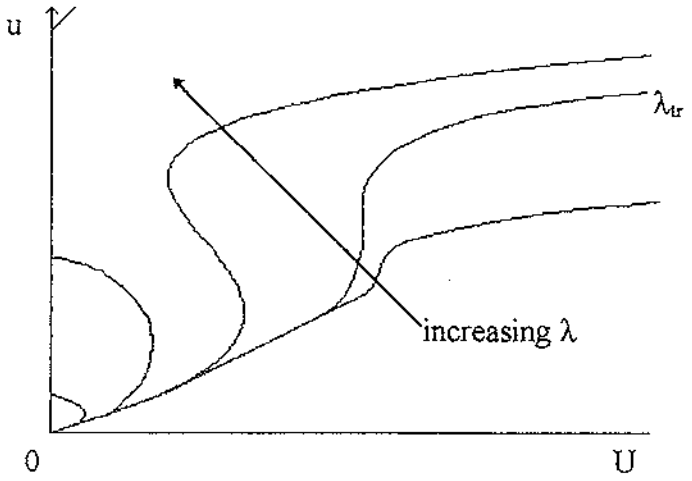

FIGURE 2.2 Bifurcation diagram for various λ in the uniform case, (2.5).

In practical situations, λ has value much greater than λ' and the variable u has values high enough to suggest that the upper branch is significant. The earlier Frank-Kamenetskii formulation does not allow an upper branch to exist under these circumstances because it does not allow multiple solutions to exist for $U = 0$: From (2.1), when U has value zero, T_a must have zero value; non-trivial solutions, u, are transformed to $\theta = \infty$. Thus, the disjoint nature of the bifurcation curve, and hence the upper branch, never appears in the classical Frank-Kamenetskii formulation.

The bifurcation diagram [8] for the sphere is shown in Figure 2.3.

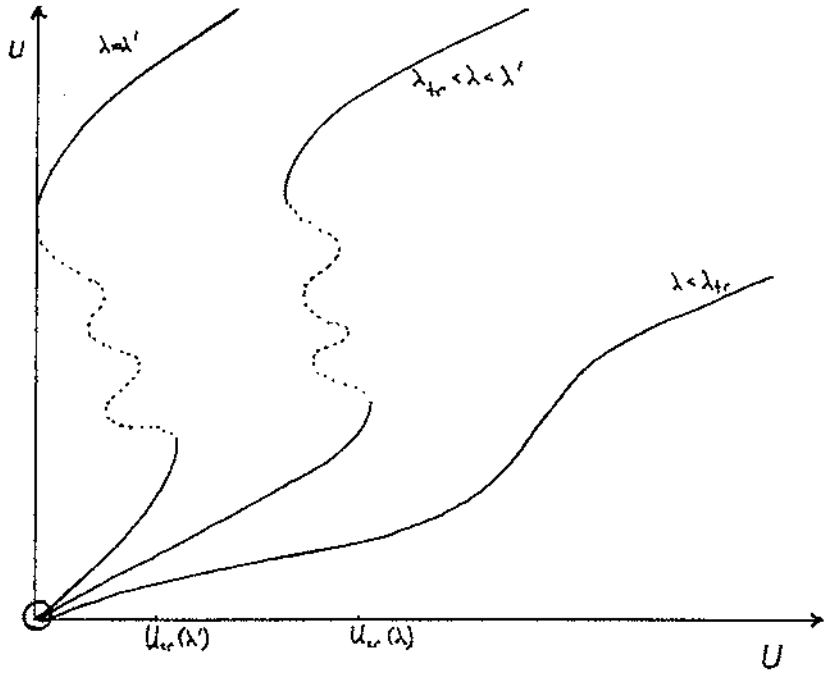

FIGURE 2.3 Bifurcation diagram for the sphere.

Later results in this thesis will show that solutions with multiplicity greater than three exist only for $\lambda > \lambda'$.

The energy distribution profile for combustion in a region, Ω, is shown in Figure 2.4. The lowest and uppermost curves are stable; the middle curve represents an unstable state. Each curve corresponds to one branch of the bifurcation diagram. For some geometries under certain conditions, there may be more than three curves on the energy distribution profile. Generally, the uppermost curve is at much greater values of u than the other curves.

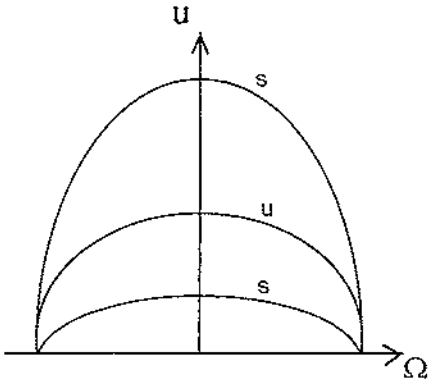

FIGURE 2.4 Energy distribution profile.

Use of the Gray Wake formulation, (2.1) - (2.3), is not only easier to apply than the Frank-Kamenetskii formulation, (1.4), but it more closely approximates the physical characteristics of thermal ignition and thermal extinction.

3 TAXONOMY OF CLASS A GEOMETRIES

3.1 Introduction

Using the Gray Wake formulation, the steady state heat balance equation for a material of arbitrary shape undergoing exothermic reaction with negligible reactant consumption is

$$\frac{d^2u}{dx^2}+\frac{j}{x}\frac{du}{dx}+\lambda\exp\left(-\frac{1}{u}\right)=0, \quad 0<x<1, \qquad u(1)=U, \quad u'(0)=0 \tag{3.1}$$

where u represents the energy across region x ($0<x<1$), λ is the Gray Wake parameter and j is the shape factor.

The shape factor j is defined by Boddington *et al* [4] as

$$j=\left(\frac{3r_0^2}{r_s^2}\right)-1,$$

where r_0 is the root mean square radius, $r_s=\frac{3V}{S}$, V is the volume of the body and S is the surface area of the body.

The aim of this study is to solve (3.1) for various values of λ and j by numerical computation. An implementation of (3.1) is developed using approximations to remove problems of overflow in the second term near x = 0. Since the energy distribution profile, shown in Figure 3.1, is reasonably flat at x = 0,

$$\frac{1}{x}\frac{du}{dx}\rightarrow\frac{d^2u}{dx^2} \quad \text{at } x=0.$$

So (3.1) can also be expressed near x = 0 as

$$(j+1)\frac{d^2u}{dx^2}+\lambda\exp\left(-\frac{1}{u}\right)=0, \quad 0<x<\varepsilon \qquad u'(0)=0. \tag{3.2}$$

The profile is symmetrical about $x = 0$, so

$$u(i=-1) = u(i=1).$$

Using a three-point approximation to $u''(x)$, with step-size h,

$$2(j+1)(u_1 - u_0) + \lambda h^2 \exp\left(-\frac{1}{u_0}\right) = 0.$$

So

$$u(i=1) = u_1 = u_0 - \frac{\lambda h^2}{2(j+1)} \exp\left(-\frac{1}{u_0}\right) = 0.$$

Using a two-point symmetric approximation to the first order derivative and a three-point symmetric approximation to the second order derivative, the problem, (3.1), becomes

$$u_1 = u_0 - \frac{\lambda h^2}{2(j+1)} \exp\left(-\frac{1}{u_0}\right)$$

$$u_i = \frac{2i-2}{2i+j-2}\left(2u_{i-1} + \left(\frac{j}{2i-2} - 1\right)u_{i-2} - \lambda h^2 \exp\left(-\frac{1}{u_{i-1}}\right)\right), \quad i = 2,3,4,\ldots,n \qquad (3.3)$$

$$u(i=n) = U.$$

3.2 j=0 Infinite slab

Equation (3.1) becomes

$$\frac{d^2u}{dx^2}+\lambda\exp\left(-\frac{1}{u}\right)=0,\quad 0<x<1,$$

$$u(1)=U,\quad u'(0)=0$$

with solution via

$$u(i=1)=u_1=u_0-\frac{\lambda h^2}{2}\exp\left(-\frac{1}{u_0}\right)=0$$

$$u_i=2u_{i-1}-u_{i-2}-\lambda h^2\exp\left(-\frac{1}{u_{i-1}}\right),\quad i=2,3,4,\ldots,n$$

$$u(i=n)=U.$$

Critical values for the slab are shown in Table 3.1. The data are included in Figure 3.10.

λ	U_{cr}	$u_{0.cr}$
100 000	0.0578812	0.0625
10 000	0.0683588	0.0748
1 000	0.0840888	0.0944
100	0.111170	0.13065
50	0.123979	0.1494
45	0.126247	0.1528
40	0.128905	0.1565
35	0.132089	0.1616
30	0.136017	0.1678
25	0.141059	0.1760
20	0.147919	0.1874
15	0.158171	0.2052
10	0.176478	0.2404
9	0.182292	0.2528
8	0.189514	0.2688
7	0.198870	0.2910
6	0.211865	0.32724
5	0.232496	0.40535
4.61836	0.245781	0.5412 - 0.5423

TABLE 3. 1 Critical values for the infinite slab.

The λ_{tr} value of 4.61836 with U_{tr} value of 0.245781 and λ' value of 6.956 agree with those of Balakrishnan [1] and Burnell [8].

Typical curves are shown in Figure 3.1.

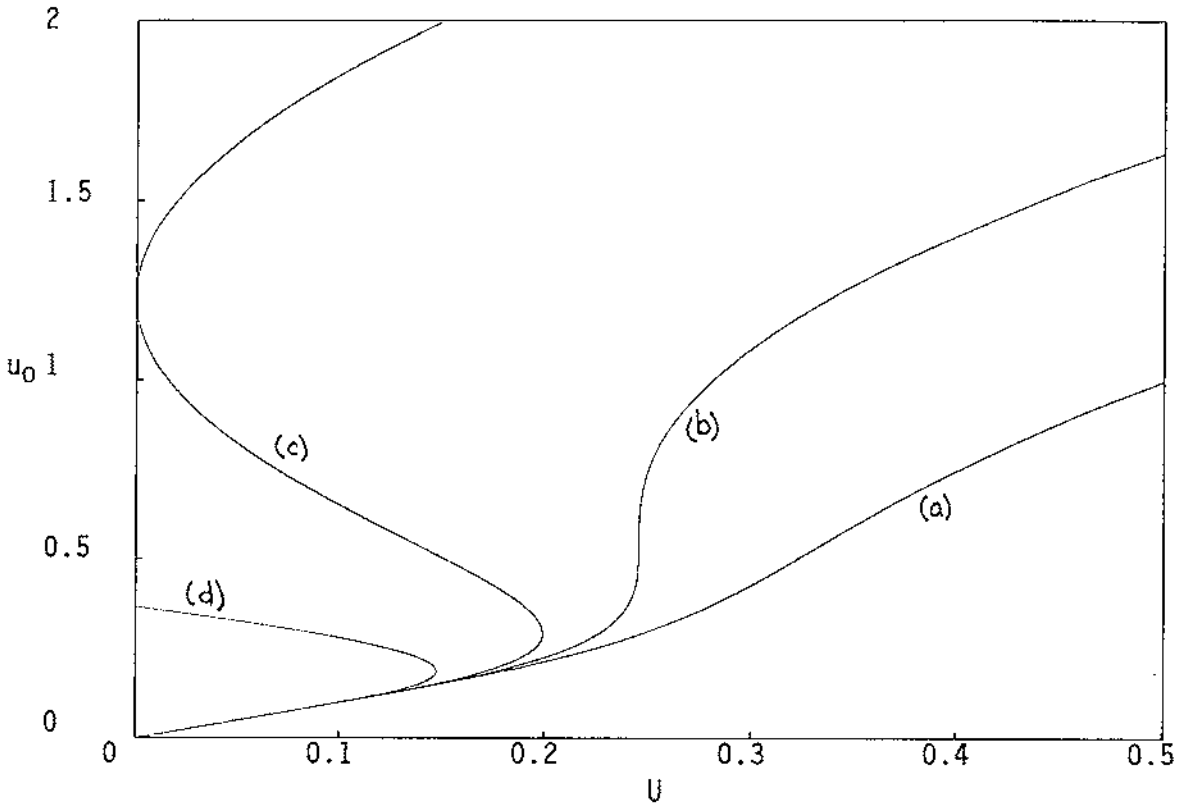

FIGURE 3. 1 Bifurcation curves for the infinite slab geometry with (a) λ = 3, (b) λ = 4.61836, (c) λ = 6.956, and (d) λ = 20.

The bifurcation curves for the infinite slab, shown in Figure 3.1, are of the form expected in Figure 2.2. As λ increases from a λ_{tr} value of 4.61836, multiple solutions exist and ignition becomes possible at $U = U_{cr}$.

3.3 j=1 Infinite cylinder

Equation (3.1) becomes

$$\frac{d^2u}{dx^2} + \frac{1}{x}\frac{du}{dx} + \lambda \exp\left(-\frac{1}{u}\right) = 0, \quad 0 < x < 1,$$

$$u(1) = U, \quad u'(0) = 0$$

with solution via

$$u_1 = u_0 - \frac{\lambda h^2}{4}\exp\left(-\frac{1}{u_0}\right)$$

$$u_i = \frac{2i-2}{2i-1}\left(2u_{i-1} + \left(\frac{1}{2i-2} - 1\right)u_{i-2} - \lambda h^2 \exp\left(-\frac{1}{u_{i-1}}\right)\right), \quad i = 2,3,4,\ldots,n$$

$$u(i=n) = U.$$

Critical values for the cylinder are shown in Table 3.2 and included in Figure 3.10.

λ	U_{cr}	$u_{0.cr}$
100 000	0.0624	0.061
10 000	0.0820	0.073
1 000	0.091944	0.107
100	0.126933	0.159
50	0.145194	0.190
45	0.148583	0.1962
40	0.152624	0.204
35	0.157572	0.213
30	0.163855	0.226
25	0.172249	0.244
20	0.184403	0.272
15	0.204814	0.328
14	0.210965	0.350
13	0.218415	0.380
12	0.227872	0.424
11	0.241361	0.552
10.99	0.241545	0.556

TABLE 3. 2 Critical values for the cylinder.

The λ_{tr} value of 10.99, with U_{tr} value of 0.2415, and λ' value of 16.84 agree with the results of other researchers, [1], [8].

Typical curves are shown in Figure 3.2.

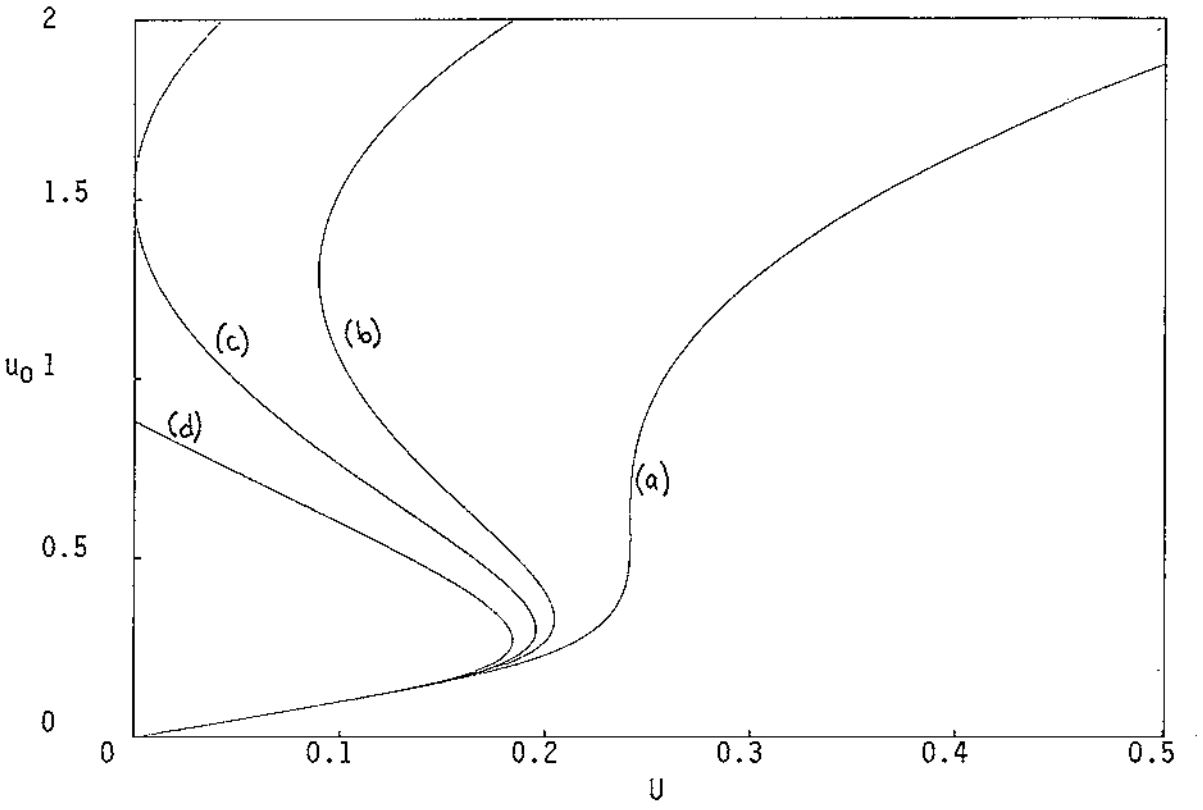

FIGURE 3. 2 Bifurcation curves for the cylinder (h = 0.01) for (a) λ = 10.99, (b) λ = 15, (c) λ = 16.84, (d) λ = 20.

The bifurcation curves for the infinite cylinder are similar to those for the infinite slab. As λ increases from a λ_{tr} value of 10.99, multiple solutions exist and ignition becomes possible at $U = U_{cr}$.

3.4 j=2 Sphere

Equation (3.1) becomes

$$\frac{d^2u}{dx^2}+\frac{2}{x}\frac{du}{dx}+\lambda\exp\left(-\frac{1}{u}\right)=0,\quad 0<x<1,$$

$$u(1)=U,\quad u'(0)=0$$

with solution via

$$u_1=u_0-\frac{\lambda h^2}{6}\exp\left(-\frac{1}{u_0}\right)$$

$$u_i=\frac{2i-2}{2i}\left(2u_{i-1}+\left(\frac{2}{2i-2}-1\right)u_{i-2}-\lambda h^2\exp\left(-\frac{1}{u_{i-1}}\right)\right),\quad i=2,3,4,\ldots,n$$

$$u(i=n)=U.$$

Critical values for the sphere are shown in Table 3.3 and included in Figure 3.10.

λ	U_{cr}	$u_{0.cr}$
100 000	0.0634971	0.0712
10 000	0.0766095	0.0880
1 000	0.097704	0.1185
100	0.139885	0.1880
50	0.164111	0.2384
45	0.168859	0.2498
40	0.174653	0.264
35	0.181969	0.282
30	0.191692	0.312
25	0.205702	0.360
20	0.229851	0.490
18.934	0.238791	0.644 - 0.654

TABLE 3. 3 Critical values for the sphere.

The λ_{tr} value of 10.99, with U_{tr} value of 0.2415, and λ' value of 16.84 agree with the results of Balakrishnan [1] and Burnell [8].

Typical curves are shown in Figure 3.3.

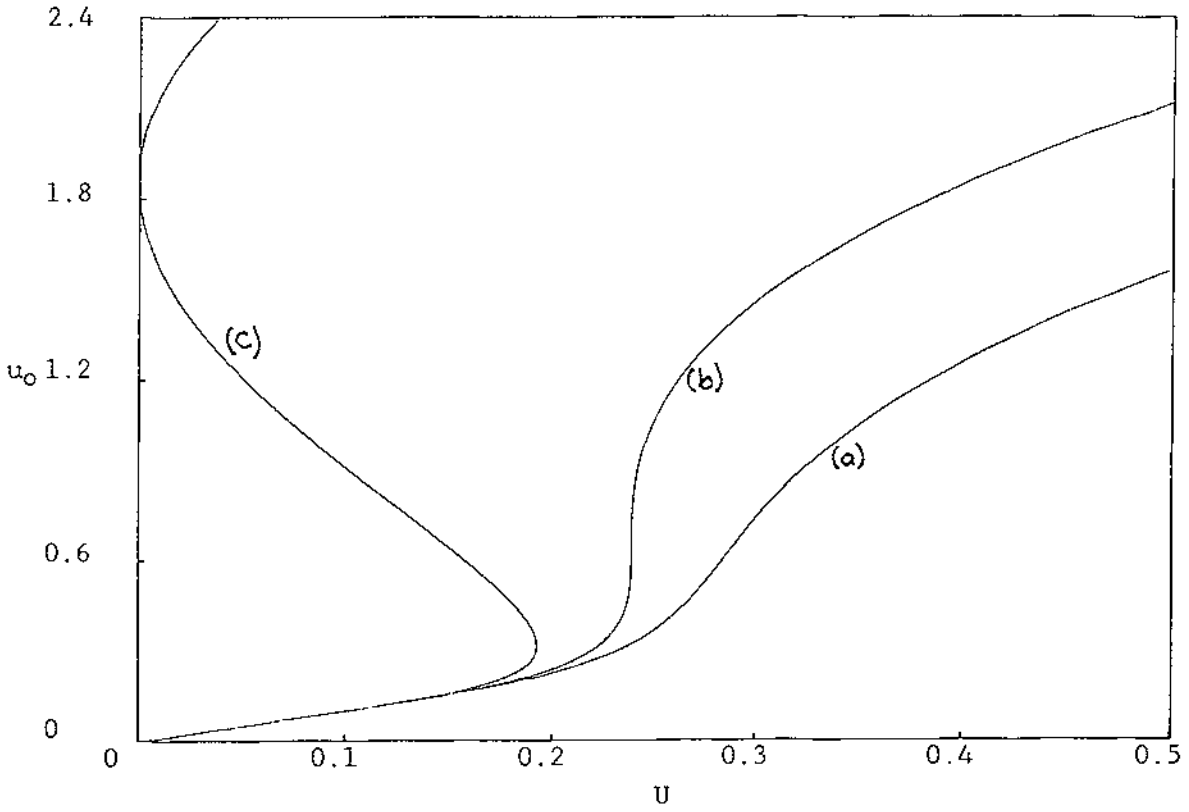

FIGURE 3. 3 Bifurcation curves for the sphere for (a) $\lambda = 15$, (b) $\lambda = 18.934$, and (c) $\lambda = 29.564$.

The bifurcation curves for the sphere at low values of λ are similar to those for the infinite slab. As λ increases from a λ_{tr} value of 10.99, multiple solutions exist and ignition becomes possible at $U = U_{cr}$. At higher values of λ, greater than $\lambda = 100\ 000$, the bifurcation curve changes form to increase the number of limit points. This is shown in Figure 3.4.

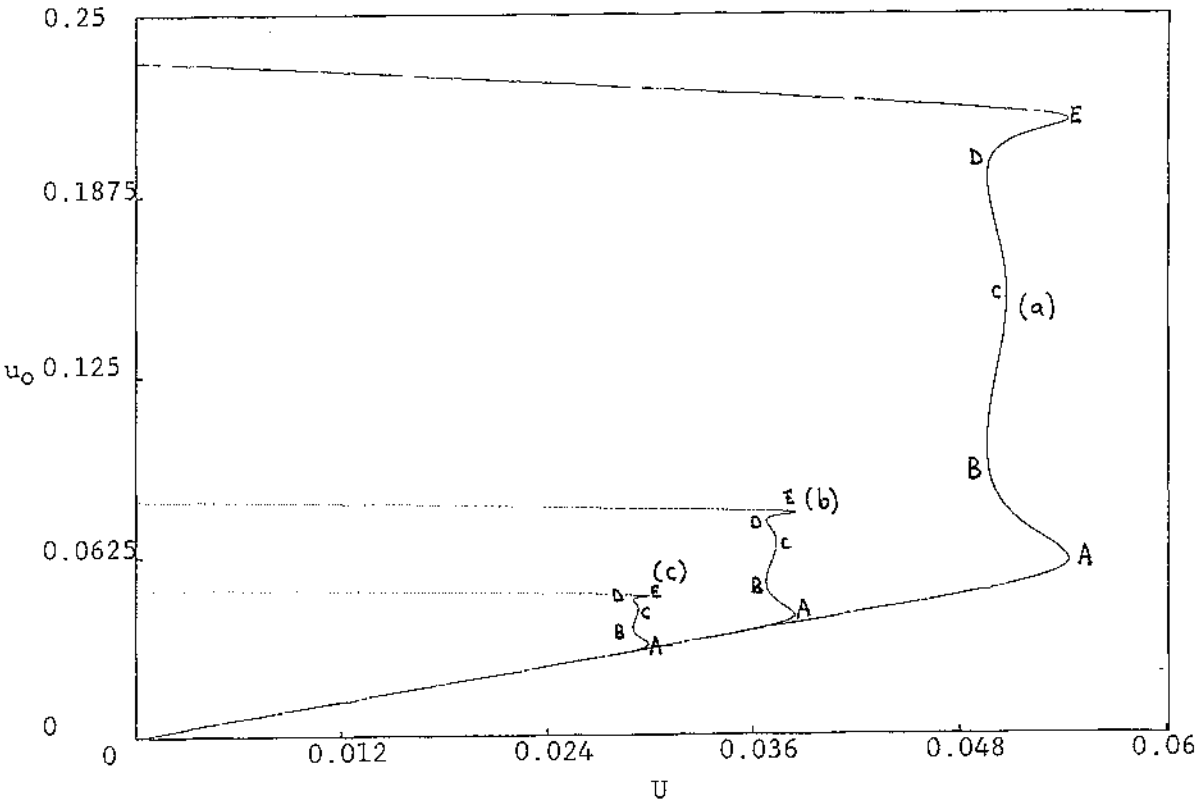

FIGURE 3. 4 Bifurcation curves for the sphere for (a) $\lambda = 1\times10^6$, (b) $\lambda = 1\times10^9$, and (c) $\lambda = 1\times10^{12}$.

The limit point positions are shown in Table 3.4. In each case, limit points A and E occur at the same U_{cr} as do limit points B and D.

	$\lambda = 1\ 000\ 000$		$\lambda = 1\ 000\ 000\ 000$		$\lambda = 1\ 000\ 000\ 000\ 000$	
	U_{cr}	$u_{0.cr}$	U_{cr}	$u_{0.cr}$	U_{cr}	$u_{0.cr}$
A	0.0544334	0.0599	0.0384699	0.0766	0.0299281	0.03148
B	0.0496205	0.0996	0.0368009	0.0525	0.0290448	0.03734
C	0.0507882	0.1519	0.0368009	0.0737	0.0293377	0.04369
D	0.0496205	0.1933	0.037392	0.066	0.0290449	0.04703
E	0.0544333	0.2133	0.0384719	0.0411	0.0299280	0.04827

TABLE 3. 4 Limit point positions for bifurcation curves for the sphere (h= 0.01).

3.5 Other geometries

The effect of increasing j beyond $j = 2$ is shown in Figure 3.5. The abrupt cessation of bifurcation curves is discussed below (see "Errors") and is caused by a combination of λ, h, and u_0. As with the class A geometries, each curve has

$$\frac{du_0}{dU} = 1, \qquad U < U_{cr}.$$

The position of limit points is given in Table 3.5. In each case, the U_{cr} value is greater than any other U value for a limit point.

$j = 2$		$j = 3$		$j = 4$		$j = 5$		$j = 6$	
U_{cr}	$u_{0,cr}$	U_{cr}	$u_{0,cr}$	U_{cr}	$u_{0,cr}$	U_{cr}	$u_{0,cr}$	U_{cr}	$u_{0,cr}$
0.0544	0.0599	0.0557	0.0624	0.0568	0.0649	0.0577	0.0677	0.0585	0.0709
0.0496	0.0996	0.0544	0.0839	0.0563	0.0846	0.0575	0.0879	0.0584	0.0935
0.0508	0.1519	0.0549	0.1348	0.0564	0.1297	0.0575	0.1516	0.0584	0.1726
0.0496	0.1933	0.0548	0.1488	0.0563	0.2021	0.0577	0.2230	0.0584	0.2156
0.0544	0.2133	0.0551	0.2020	0.0564	0.2202	0.0483	0.2436	0.0585	0.2265
		0.0543	0.2469	0.0563	0.2369	0.0577	0.2679		
		0.0556	0.2575	0.0564	0.2619	0.0575	0.2916		
						0.0577	0.3011		

TABLE 3. 5 Limit points for geometries with $j \geq 2$ for $\lambda = 1\times10^6$ ($h = 0.01$).

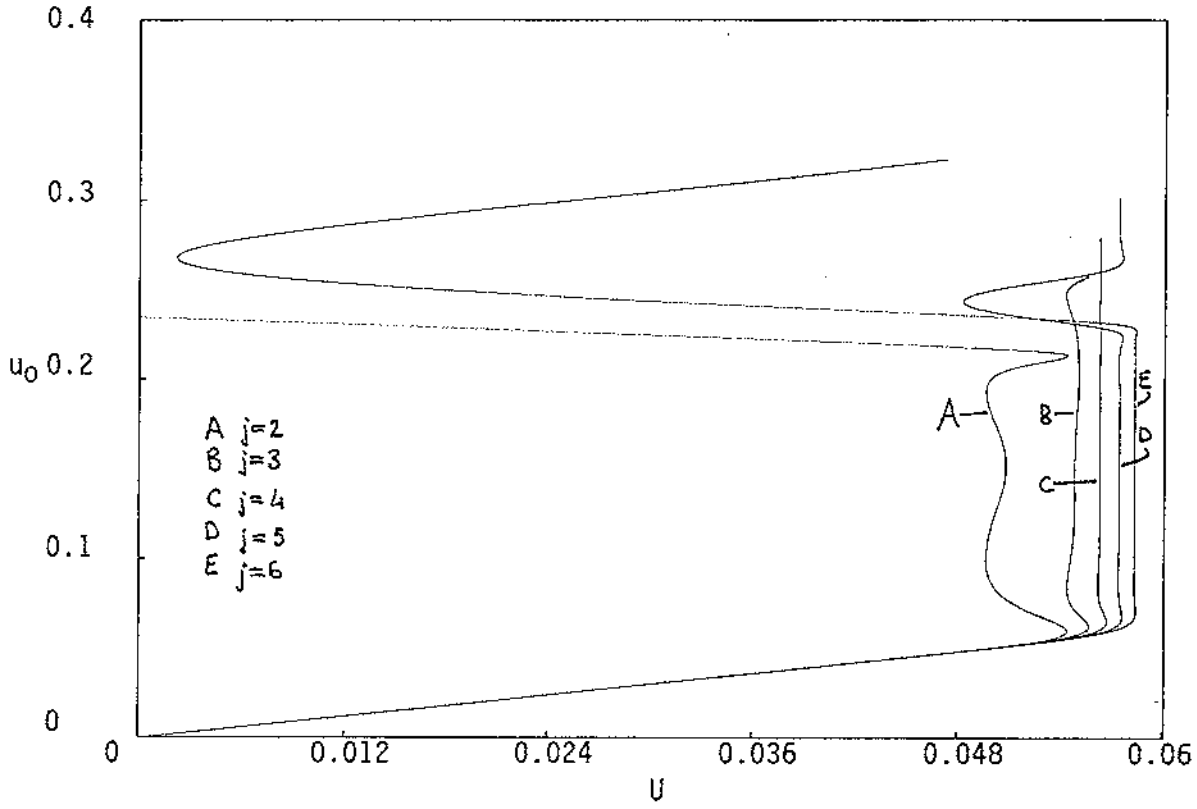

FIGURE 3. 5 Bifurcation curves for the geometries corresponding to j = 2, 3, 4, 5 and 6 for $\lambda = 1\times10^6$ ($h = 0.01$).

At $j = 1$, there is only one limit point for bifurcation curves corresponding to $\lambda > \lambda'$; at $j = 2$, there are at least five such limit points. Between $j = 1$ and $j = 2$, the number of limit points increases from one to three to five. This can be seen in Figure 3.6.

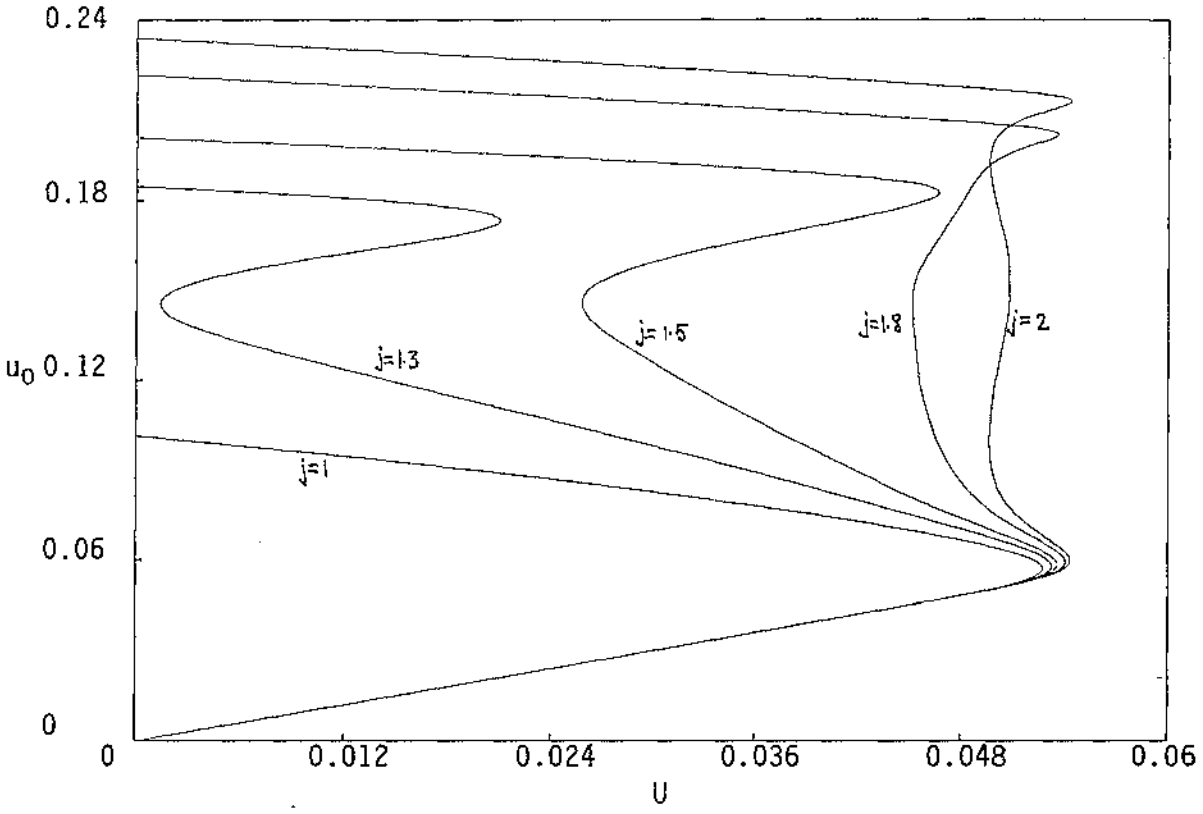

FIGURE 3. 6 Bifurcation curves for the geometries corresponding to j = 1, 1.3, 1.5, 1.8 and 2 for $\lambda = 1\times10^6$ (h = 0.01).

3.6 Upper branch

When $\lambda > \lambda'$, $U = 0$ occurs for at least two values of u_0, one of which is always $u_0 = 0$. Another value of u_0, for which U has value 0, occurs at values which are dependent on geometry and on λ. This point represents one end of the upper stable branch of the bifurcation curve, and can be termed the "re-emergence" point. Typical values of re-emergence points are given in Table 3.6.

The re-emergence u_0 value

$$u_0(U=0) \to \frac{\lambda}{2(j+1)} - \lambda h^2.$$

From (3.3),

$$\text{as } u_i \to U = 0, \quad \lambda h^2 \exp\left(-\frac{1}{u_{i-1}}\right) \to \lambda h^2$$

$$\frac{j}{2i-2} - 1 \to -1.$$

So,

$$2u_{i-1} = u_{i-2} + \lambda h^2.$$

λ	$j = 0$ (infinite slab)	$j = 1$ (infinite cylinder)	$j = 2$ (sphere)
30	13.58	5.68	2.22
50	23.60	10.78	6.26
100	48.61	23.34	14.76
1 000	498	248.38	164.84
10 000	4998	2498.50	1665.00
100 000	49999	24998.40	16664.90

TABLE 3. 6 Re-emergence points.

The trend is evident in Figure 3.7.

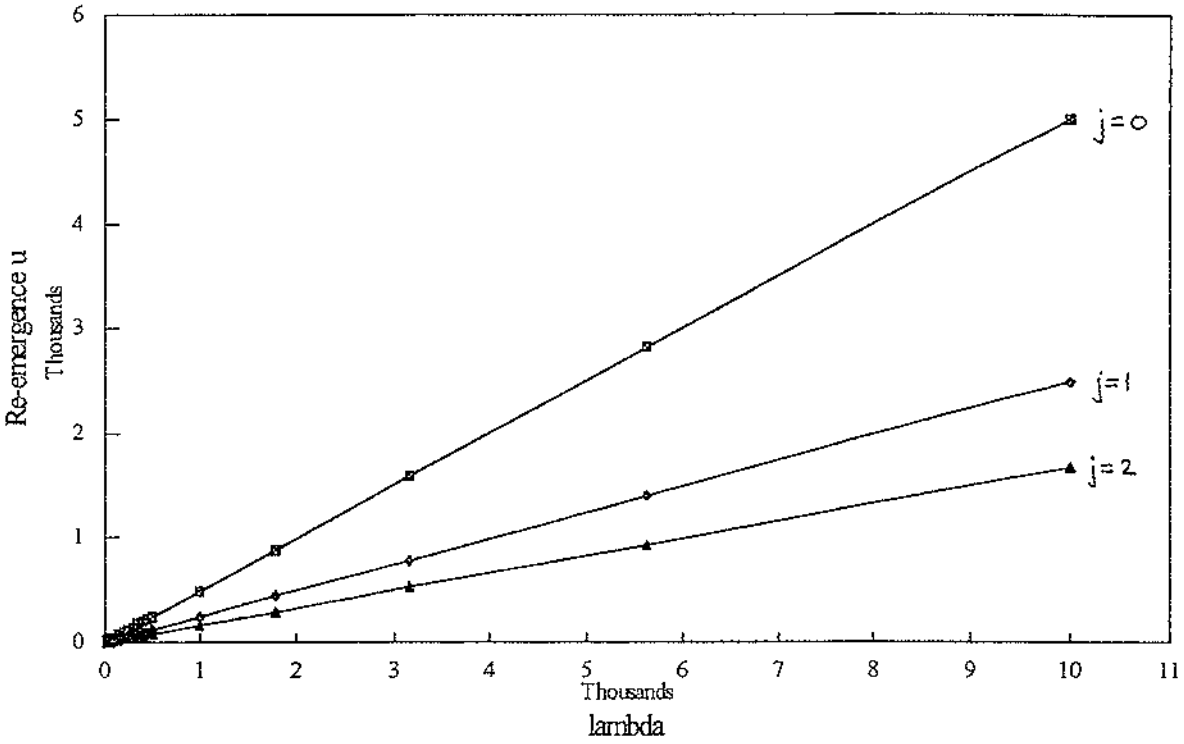

FIGURE 3. 7 Re-emergence value of u_0 as a function of λ.

3.7 Errors

3.7.1 Computation precision

All computations above have been made using computer programs written in Borland C++ version 3.1. Such calculations were conducted using long doubles with 19-digit precision. Each stage was exercised within a range of 3.4E-4932 and 1.1E4932. The value of λ is stored as a double precision 15-digit variable with range 1.7E-308 to 1.7E308, and is promoted to long double precision during computation.

At each step, truncation and rounding errors may occur.

3.7.2 Rounding

The most likely region for rounding errors to occur is in the exponential term $\exp\left(-\frac{1}{u_{i-1}}\right)$. Such errors can be avoided by introduction of a scaling factor, F, as in

$$u_i = \frac{2i-2}{2i+j-2}\left(2u_{i-1} + \left(\frac{j}{2i-2} - 1\right)u_{i-2} - \lambda h^2 \exp(-F)\exp\left(F - \frac{1}{u_{i-1}}\right)\right), \quad i = 2,3,4,\ldots,n$$

Application of such a scaling factor results in no change in limit points or in the shape of curve. Thus, rounding errors do not play a significant rôle in the calculation of U.

3.7.3 Truncation

The most likely sector for truncation errors to occur is the casting from one data type to another. No such errors occur in this study because all casts are either from float or double precision reals into long doubles, where no truncation occurs, or from integer into long double (real) precision, where there can be no loss of precision.

3.7.4 Swamping

The term $\lambda h^2 \exp\left(-\frac{1}{u_{i-1}}\right)$ in (3.3) is made smaller by reducing the step-size and made larger by increasing λ. As the term gets larger, it "swamps" the rest of the expression for U, resulting in a negative U value. This occurs when

$$\lambda h^2 \exp\left(-\frac{1}{u_{i-1}}\right) >> 2u_{i-1} + \left(\frac{j}{2i-2} - 1\right)u_{i-2}.$$

So, for any combination of j, u_{i-1} and u_{i-2}, there is an upper limit to λ and to h for which meaningful values of U can be obtained.

3.7.5 Variation of *h*

The variable u_1 in (3.3) is made negative when

$$\frac{\lambda h^2}{2(j+1)} \exp\left(-\frac{1}{u_0}\right) > u_0$$

which, for $j = 3$, $h = 0.005$ and $\lambda = 1\times10^6$, occurs at $u_0 = 0.61563$. Thus, the bifurcation curve for the above combination of variables stops abruptly at $u_0 = 0.61563$. When h has value 0.01, $u_1 < 0$ at $u_0 = 0.258$. Although each curve stops at different values of u_0, they have the same U_{cr} value.

When the step-size, h, in the finite differences approximation is diminished, more steps are required from $x = 0$ to $x = 1$. Errors incurred in each step can accumulate resulting in a greater inherent error in U at smaller h. The effect of this can be seen in Figure 3.5. For $\lambda = 500\ 000$, as h is diminished below 0.01, the number of limit points is reduced. For all values of h, the U_{cr} value is unchanged at 0.05686. For $h = 0.01$ and $h = 0.02$, the upper limit point also corresponds to $U = 0.0586$.

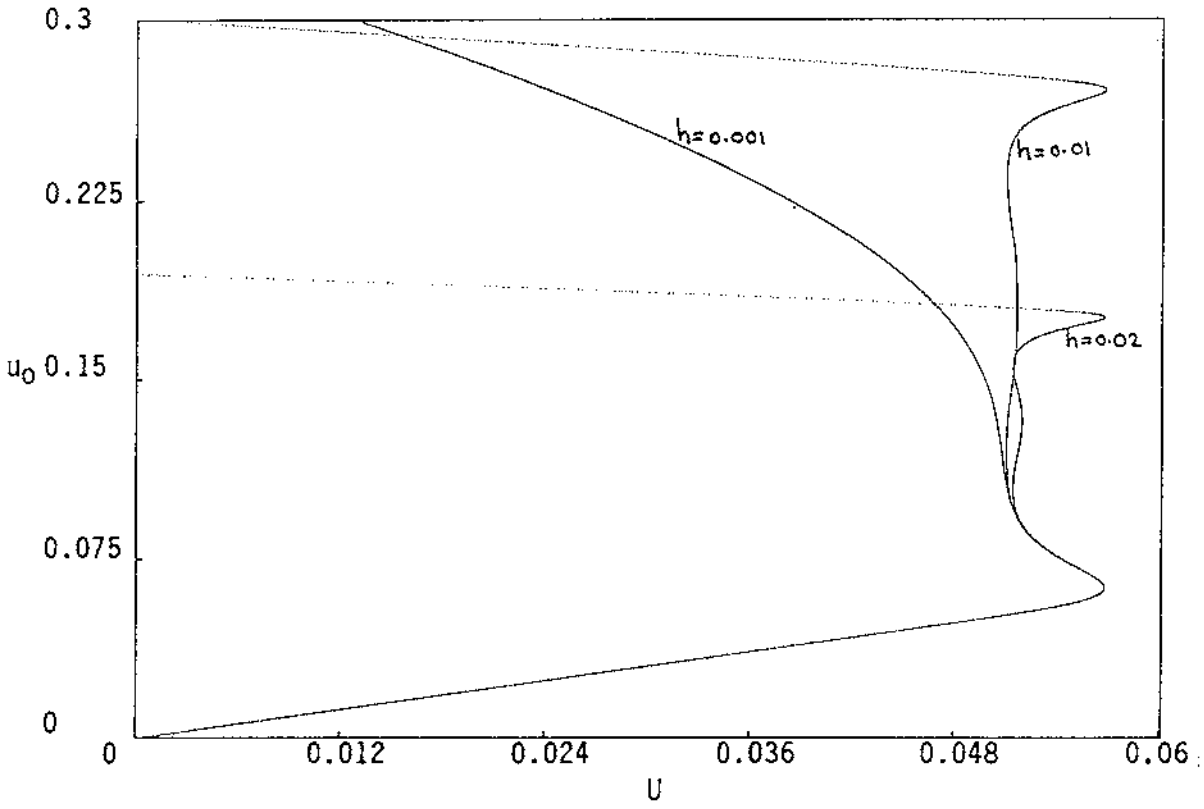

FIGURE 3. 8 The effect of changing h on the bifurcation curve for $\lambda = 500\ 000$.

As noted above, varying h changes the relationship between the terms in the expression for U. This has greater effect at higher values of λ. In Figure 3.8, with $\lambda = 500\ 000$, diminishing h induces errors; in Figure 3.9, with $\lambda = 1\times10^3$, diminishing h results in lesser changes in the bifurcation curve.

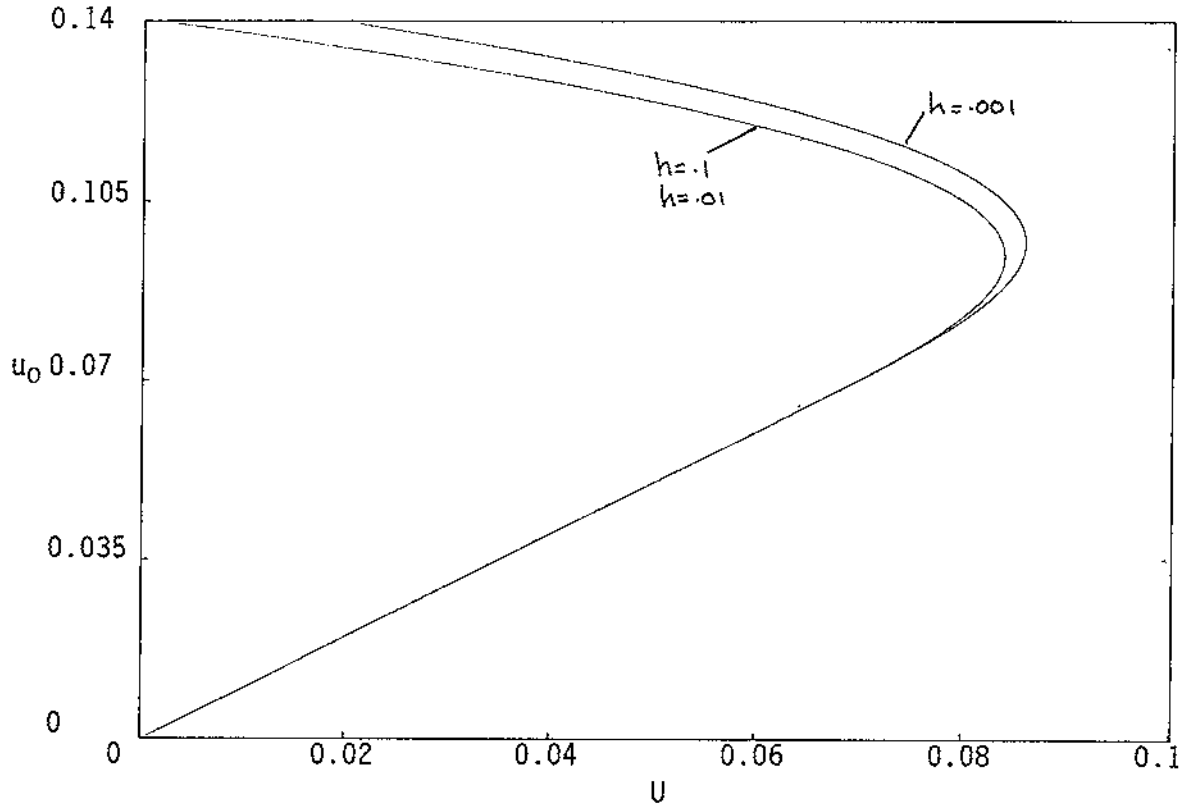

FIGURE 3. 9 The effect of changing h on the bifurcation curve for $\lambda = 1000$.

3.8 Summary

The Gray Wake formulation of the steady state heat balance equation for exothermic reaction with negligible reactant consumption can be described via finite differences approximations of both first- and second-order derivatives as

$$u_1 = u_0 - \frac{\lambda h^2}{2(j+1)} \exp\left(-\frac{1}{u_0}\right)$$

$$u_i = \frac{2i-2}{2i+j-2}\left(2u_{i-1} + \left(\frac{j}{2i-2} - 1\right)u_{i-2} - \lambda h^2 \exp\left(-\frac{1}{u_{i-1}}\right)\right), \quad i = 2,3,4,\ldots,n$$

$$u(i=n) = U$$

with step-size h.

As the shape factor, j, is increased above $j = 1$, the number of limit points increases to five for $\lambda \geq 1\times10^{6}$.

For all geometries and all values of λ,

$$\frac{du_0}{dU} = 1, \qquad U < U_{cr}.$$

The lower limit point is always at the maximum value of U.

For $\lambda > \lambda'$, the upper stable branch of the bifurcation curve appears to include the point $(U, u_0) = \left(0, \frac{\lambda}{2(j+1)} - \lambda h^2\right)$.

At high values of λ, errors become significant. In general, the bifurcation curves have the form described by other researchers.

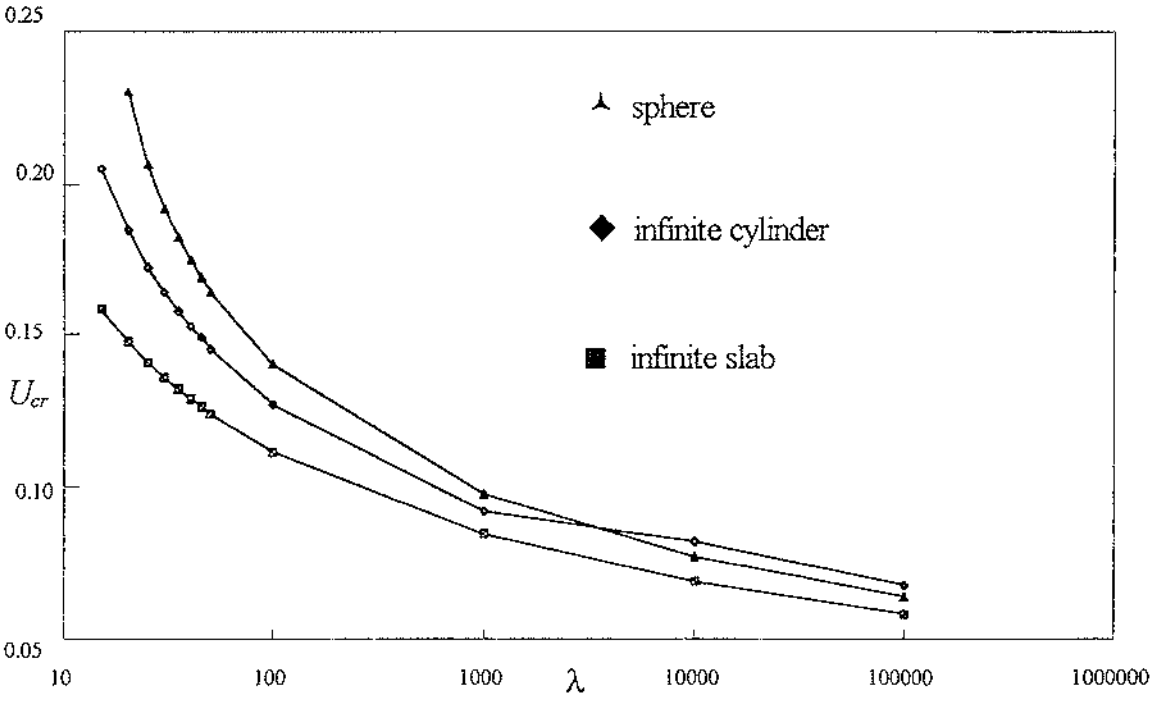

FIGURE 3. 10 U_{cr} values for the infinite slab, infinite cylinder and sphere.

4 Use of Approximations

4.1 Introduction

Using the Gray Wake formulation for combustion in an infinite slab, the energy balance equation is

$$\frac{d^2u}{dx^2} + \lambda \exp\left(-\frac{1}{u}\right) = 0 \quad \text{in } \Omega \tag{4.1}$$

with boundary condition

$$u = u_a \text{ on } \partial\Omega,$$

where u is the dimensionless temperature of an exothermically reacting material in bounded domain Ω in R^n with smooth boundary $\partial\Omega$ and λ is the dimensionless parameter,

$$\lambda = \frac{\sigma QARa_0^2}{kE},$$

where s is the density of material, Q the exothermicity, A the Arrhenius frequency factor, R the universal gas constant, a_0 some measure of length, k the thermal conductivity, and E the activation energy.

The heat balance equation for combustion in the slab geometry can be written as

$$\frac{d^2u}{dx^2} + \lambda \exp\left(-\frac{1}{u}\right) = 0, \quad -1 < x < 1 \tag{4.2}$$

with boundary condition $u = u_a, \quad x = \pm 1$

where u = RT/E.

This heat balance equation cannot be solved analytically. Approximation is possible via the exponential term by replacing the u by an average value across the region, u_{av}, or by a maximum value in the region, u_{max}.

4.2 Approximation by average *u*

When the average value of u, u_{av}, is used to approximate the u in the exponential term of (4.2), the equation becomes

$$\frac{d^2u}{dx^2} + \lambda \exp\left(-\frac{1}{u_{av}}\right) = 0$$

$$u = u_a, \quad x = \pm 1$$

Rearranging,

$$u''(x) = -\lambda \exp\left(-\frac{1}{u_{av}}\right)$$

$$\equiv -C \qquad \text{constant } C.$$

Integrating,

$$u(x) = -\frac{C}{2}x^2 + Ax + B.$$

By symmetry, $A = 0$. From the boundary condition, $u(1) = U$, so

$$u_a = -\frac{C}{2} + B$$

$$\Rightarrow \qquad B = \frac{C}{2} + u_a$$

$$\Rightarrow \qquad u(x) = \frac{C}{2}\left(1 - x^2\right) + u_a.$$

4.2.1 Construction of the curve

The curve of U versus $u_{max} = u(0)$ is created by calculating values for each of U and $u(0)$ from values of u_{av} and plotting these against each other as follows:

$$\begin{aligned} u_{av} &= \int_0^1 u(x)\,dx \\ &= \frac{C}{2}\left(1-\frac{1}{3}\right)+u_a \\ &= \frac{\lambda}{2}\exp\left(-\frac{1}{u_{av}}\right)\cdot\frac{2}{3}+u_a \\ &= \frac{\lambda}{3}\exp\left(-\frac{1}{u_{av}}\right)+u_a \\ u_a &= u_{av}-\frac{\lambda}{3}\exp\left(-\frac{1}{u_{av}}\right). \end{aligned} \tag{4.3}$$

Also,

$$\begin{aligned} u(x) &= \frac{\lambda}{2}\left(1-x^2\right)\exp\left(-\frac{1}{u_{av}}\right)+u_a \\ u(0) &= u_0 \\ u_0 &= \frac{\lambda}{2}\exp\left(-\frac{1}{u_{av}}\right)+u_a \\ u_0 &= u_{av}-\frac{\lambda}{3}\exp\left(-\frac{1}{u_{av}}\right)+\frac{\lambda}{2}\exp\left(-\frac{1}{u_{av}}\right) \\ &= u_{av}+\frac{\lambda}{6}\exp\left(-\frac{1}{u_{av}}\right). \end{aligned} \tag{4.4}$$

Thus, for any given value of u_{av},

$$u_a = u_{av}-\frac{\lambda}{3}\exp\left(-\frac{1}{u_{av}}\right) \tag{4.3}$$

$$u_0 = u_{av}+\frac{\lambda}{6}\exp\left(-\frac{1}{u_{av}}\right) \tag{4.4}$$

4.2.2 Calculation of critical values

The value of du_a/du_0 is calculated as follows:

$$u_a = u_{av} - \frac{\lambda}{3}\exp\left(-\frac{1}{u_{av}}\right)$$

$$\frac{du_a}{du_{av}} = 1 - \frac{\lambda}{3}\left[\exp\left(-\frac{1}{u_{av}}\right)\right]\frac{1}{u_{av}^2}$$

$$u_0 = u_{av} + \frac{\lambda}{6}\exp\left(-\frac{1}{u_{av}}\right)$$

$$\frac{du_0}{du_{av}} = 1 + \frac{\lambda}{6}\left[\exp\left(-\frac{1}{u_{av}}\right)\right]\frac{1}{u_{av}^2}$$

So $$\frac{du_a}{du_0} = \frac{1-2y}{1+y} \qquad (4.5)$$

where $$y = \frac{\lambda \exp\left(-\frac{1}{u_{av}}\right)}{6u_{av}^2}. \qquad (4.6)$$

Of interest is the point on the curve at which $du_a/du_0 = 0$. The value of U at which this occurs is termed U_{cr}. The fold bifurcation occurs at this point.

4.2.3 Results

Typical results are shown in Figures 4.2 - 4.7. The curves are consistent with earlier results in which a characteristic value of λ, λ_{tr}, can be identified as the lowest value of λ at which du_a/du_0 calculated above has value zero. For λ greater than λ_{tr}, a fold bifurcation point occurs at $U = U_{cr}$. When λ is greater than λ_{tr}, there are multiple solutions and the system is able to migrate to the upper branch from the stable lower branch, resulting in thermal ignition; no such multiple solutions exist for λ less than λ_{tr}. The variation of U_{cr} with λ is shown in Figure 4.8. Values of U_{cr} are shown in Table 4.1. The maximum value of U_{cr} is 0.249967 which occurs for $\lambda_{tr} = 5.542517$.

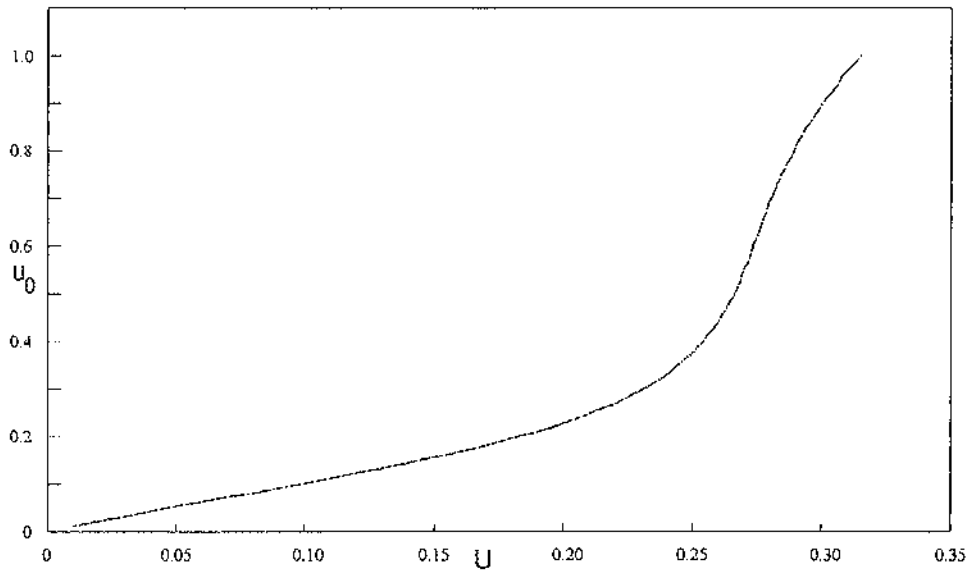

FIGURE 4.2 The u_0 versus U curve for $\lambda = 5$, using the approximation of u by u_{av}, the average value of u. The u_{av} values range from 0 to 0.77.

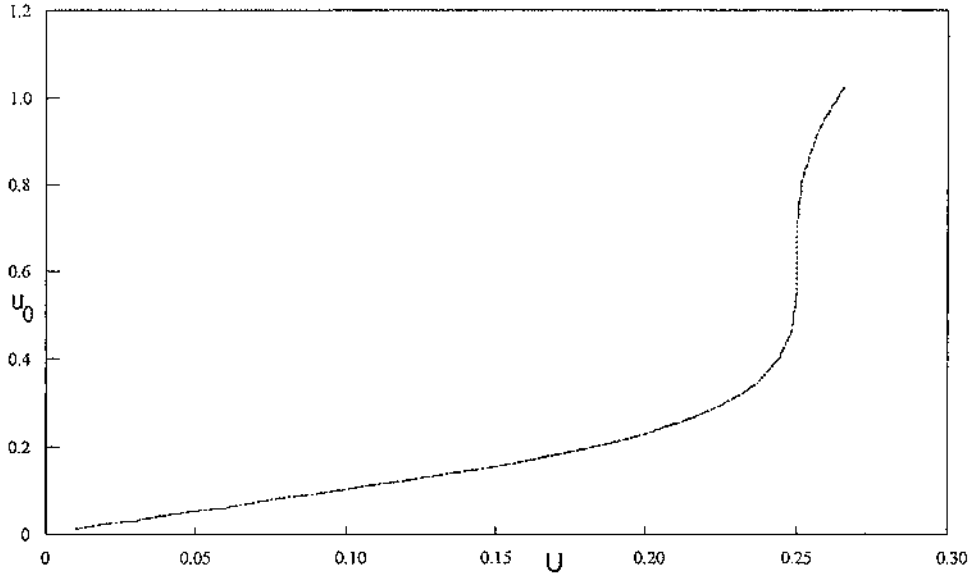

FIGURE 4.3 The u_0 versus U curve for $\lambda = 5.542517$, using the approximation of u by u_{av}, the average value of u. The u_{av} values range from 0 to 0.77. At U=0.249967, the curve is vertical, indicating that $\lambda_{tr} = 5.542517$. A vertical section occurs only when $\lambda = \lambda_{tr}$.

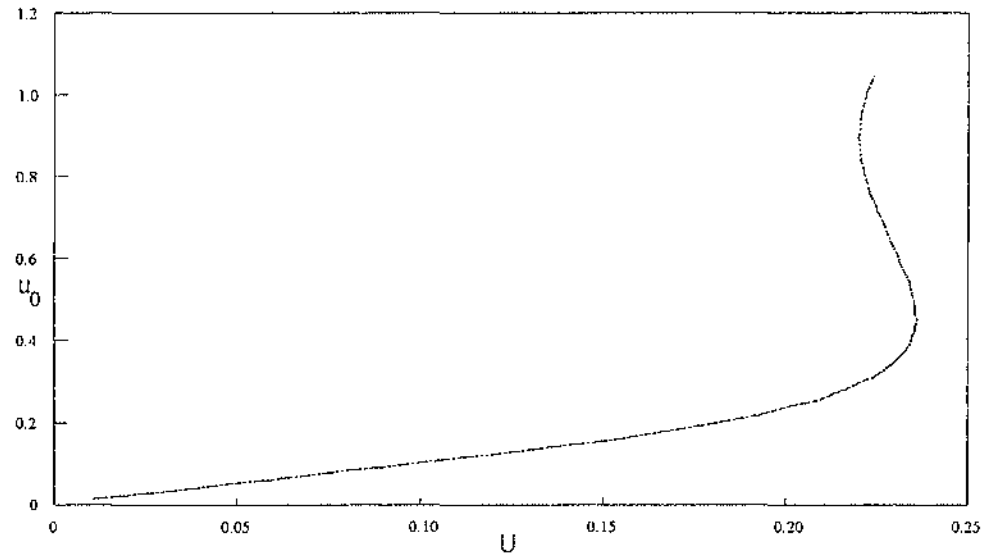

FIGURE 4.4 The u_0 versus U curve for $\lambda = 6$, using the approximation of u by u_{av}, the average value of u. The u_{av} values range from 0 to 0.77. In this case, $U_{cr} = 0.236$

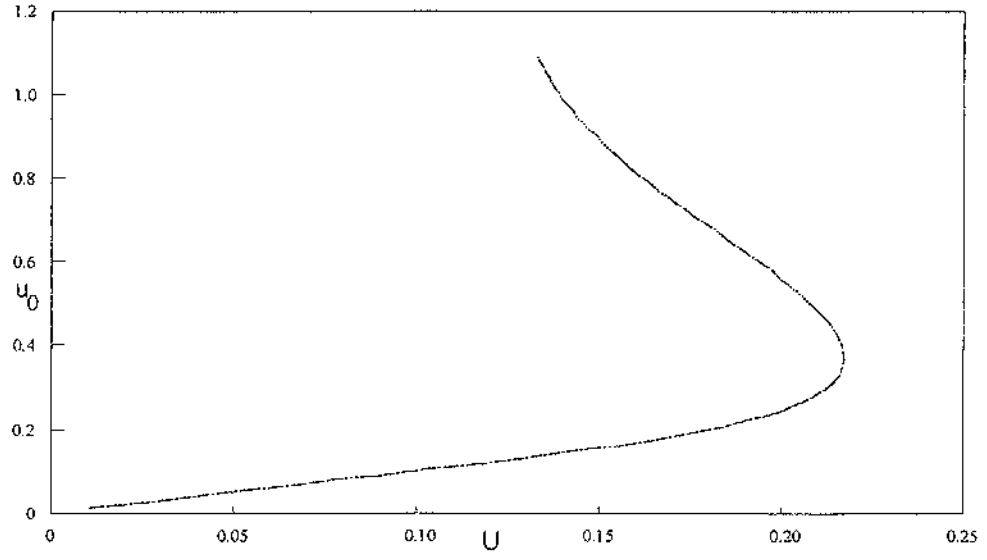

FIGURE 4.5 The u_0 versus U curve for $\lambda = 7$, using the approximation of u by u_{av}, the average value of u. The u_{av} values range from 0 to 0.77. In this case, $U_{cr} = 0.2174$.

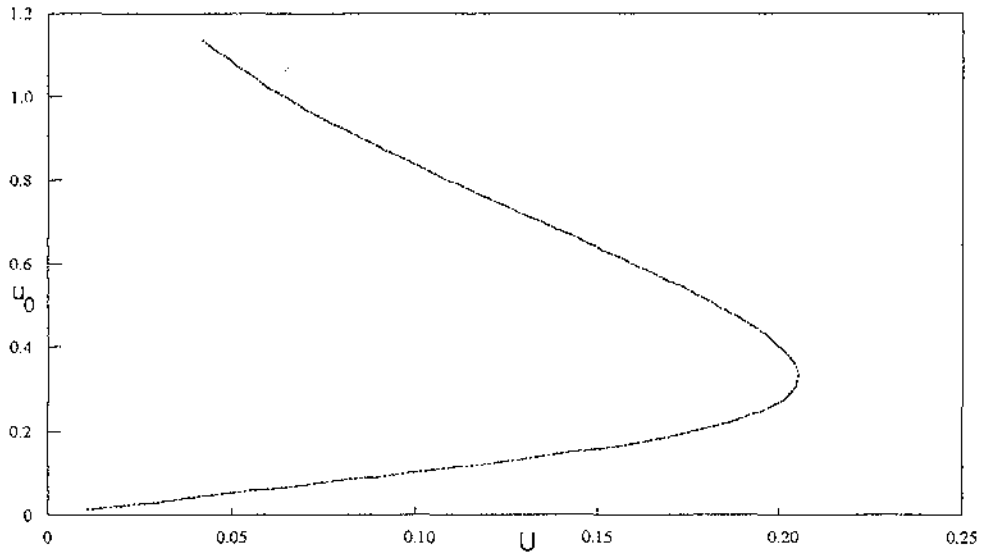

FIGURE 4.6 The u_0 versus U curve for $\lambda = 8$, using the approximation of u by u_{av}, the average value of u. The u_{av} values range from 0 to 0.77. In this case, U_{cr} is 0.205.

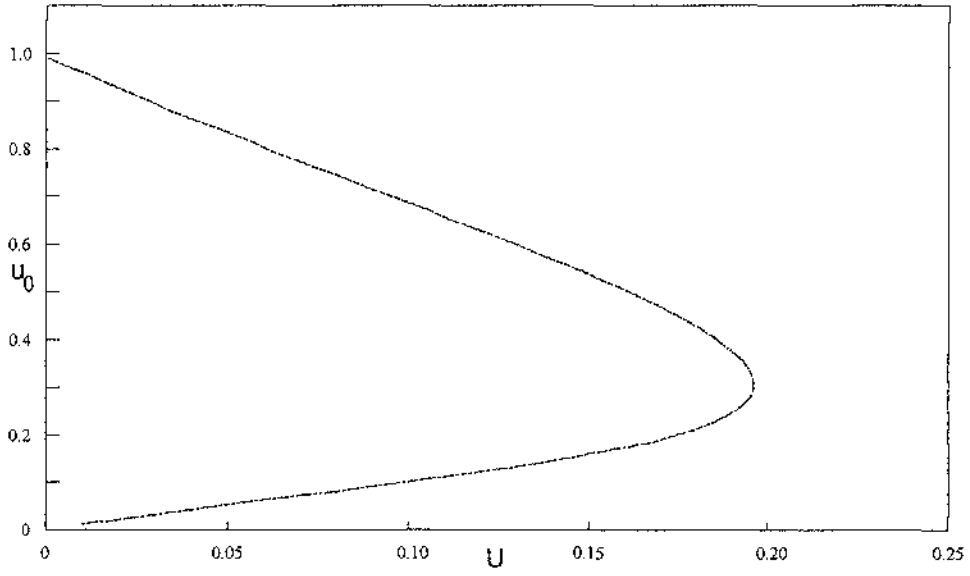

FIGURE 4.7 The u_0 versus U curve for $\lambda = 9$, using the approximation of u by u_{av}, the average value of u. The u_{av} values range from 0 to 0.66. The value of U_{cr} is 0.196.

λ	U_{cr}	$u_{0,cr}$
5.542517	0.249967	0.500
5.55	0.249645	0.485
6	0.236073	0.453
7	0.217480	0.370
8	0.205205	0.329
9	0.196116	0.302
10	0.188979	0.284
15	0.167289	0.234
20	0.155528	0.211
25	0.147784	0.196
30	0.142142	0.185
35	0.137782	0.179
40	0.134253	0.171
45	0.131330	0.167
50	0.128832	0.162
55	0.126678	0.159
60	0.124796	0.157
65	0.123104	0.153
70	0.121597	0.151
75	0.120228	0.148
80	0.118993	0.148
85	0.117847	0.145
90	0.116798	0.144
95	0.115811	0.142
100	0.114909	0.141

TABLE 4.1 Variation of U_{cr} and of $u_{0,cr}$ with λ for

$$\frac{d^2u}{dx^2} + \lambda \exp\left(-\frac{1}{u_{av}}\right) = 0, \quad -1 < x < 1$$

$$u(x) = u_a, \quad x = \pm 1$$

where U_{cr} is the largest value of U at which multiple solutions occur, $u_{0,cr}$ is the corresponding u_0 value, and u_{av} is the average value of $u(x)$. The number of significant figures reported represents the precision with which individual measurements were able to be made.

The curves in Figures 4.2 - 4.7 appear similar at low values of both u_0 and U. This is to be expected from (4.3) and (4.4) since small values of u_0 and U arise from small values of u_{av}. In (4.6), when u_{av} is small,

$$y \cong \frac{\lambda \exp(0)}{6u_{av}^2}$$

$$<< 1$$

so, substituting into (4.5),

$$\frac{du_a}{du_0} = \frac{1-2y}{1+y}$$

$$\approx 1$$

regardless of λ. For this reason, all the curves have slope close to 1, initially. There appears to be a limiting value of U_{cr} of 0.25.

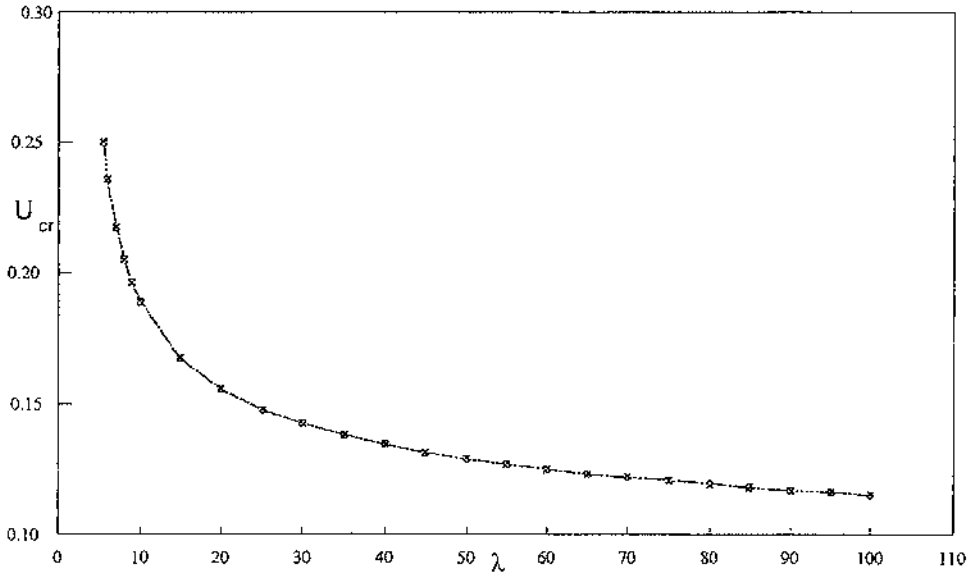

FIGURE 4.8 Variation of U_{cr} with λ for

$$\frac{d^2u}{dx^2} + \lambda \exp\left(-\frac{1}{u_{av}}\right) = 0, \quad -1 < x < 1$$

$$u(x) = u_a, \quad x = \pm 1$$

where U_{cr} is the largest value of U at which multiple solutions occur, and u_{av} is the average value of $u(x)$. Data for this curve are contained in Table 4.1. Values of U_{cr} appear to approach a limit of 0.25; the minimum value of λ is 5.542517.

4.3 Approximation by maximum *u*

When the maximum value of u, u_{max}, is used to approximate the u in the exponential term of (4.2), the heat balance equation for combustion in the slab geometry becomes

$$\frac{d^2u}{dx^2} + \lambda \exp\left(-\frac{1}{u_{max}}\right) = 0$$
$$u(x) = u_a \quad x = \pm 1$$

where u_{max} is the maximum value of $u(x)$ for $-1 < x < 1$.

4.3.1 Construction of the curve

From the curve in Figure 4.1, it can be seen that by symmetry, the maximum value of $u(x)$, u_{max}, occurs at $x = 0$. Thus the equation can be re-written as

$$u'' = -\lambda \exp\left(-\frac{1}{u_{max}}\right).$$

Integrating,

$$u(x) = u_a + \frac{\lambda}{2}\left(\exp\left(-\frac{1}{u_{max}}\right)\right)\left(1 - x^2\right).$$

Substituting,

$$u(0) = u_a + \frac{\lambda}{2} e^{-\frac{1}{u_0}}$$
$$= u_0$$
$$u_a = u_0 - \frac{\lambda}{2} e^{-\frac{1}{u_0}}. \qquad (4.7)$$

4.3.2 Calculation of critical values

From (4.7), the value of du_a/du_0 can be calculated as

$$\frac{du_a}{du_0} = 1 - \frac{\lambda}{2}\frac{\exp\left(-\frac{1}{u_0}\right)}{u_0^2}$$
$$= 1 + \frac{u_a - u_0}{u_0^2}. \qquad (4.8)$$

This has value zero at $u = U_{cr}$, the fold bifurcation point.

4.3.3 Results

Typical curves are shown in Figures 4.9-4.14. As λ decreases, the critical value, U_{cr} approaches a minimum of 0.249648. The corresponding value of λ at this point is 3.7. This is the λ_{tr} value. For λ greater than 3.7, there exist multiple solutions to the heat balance equation; the system is able to jump to the higher less stable solution, resulting in thermal ignition. The variation of U_{cr} with λ is shown in Table 4.2 and in Figure 4.15.

The closeup views of the critical region (Figures 4.10 - 4.12) show the marked changes as λ moves from $\lambda_{tr} - \varepsilon$ to $\lambda_{tr} + \varepsilon$, small ε. For $\lambda < \lambda_{tr}$, multiple solutions do not exist. The maximum value of U_{cr} is 0.25000 which occurs for $\lambda_{tr} = 3.69451$.

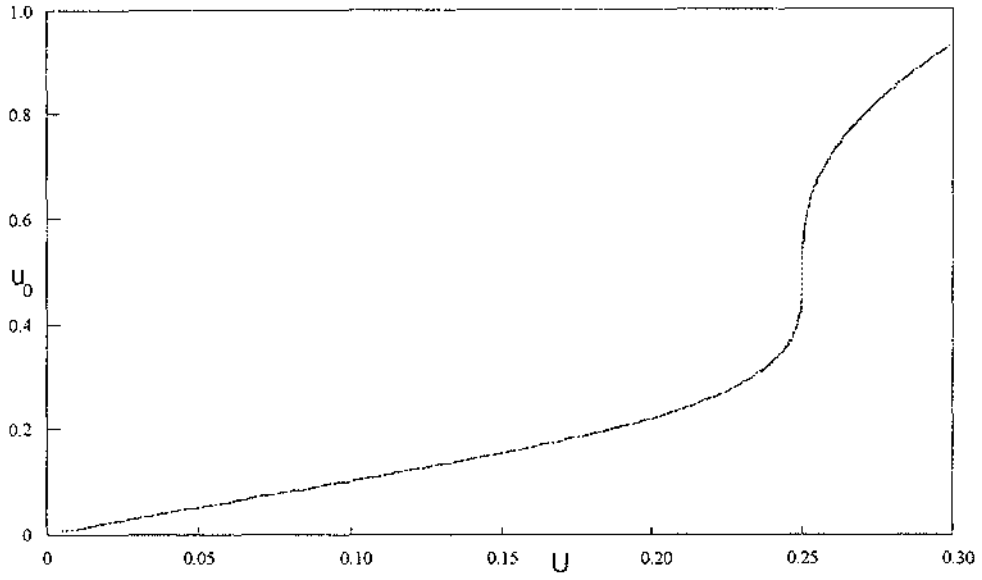

FIGURE 4.9 The u_0 versus U curve for $\lambda = 3.694$, using the approximation of u by u_{max}, the maximum value of u.

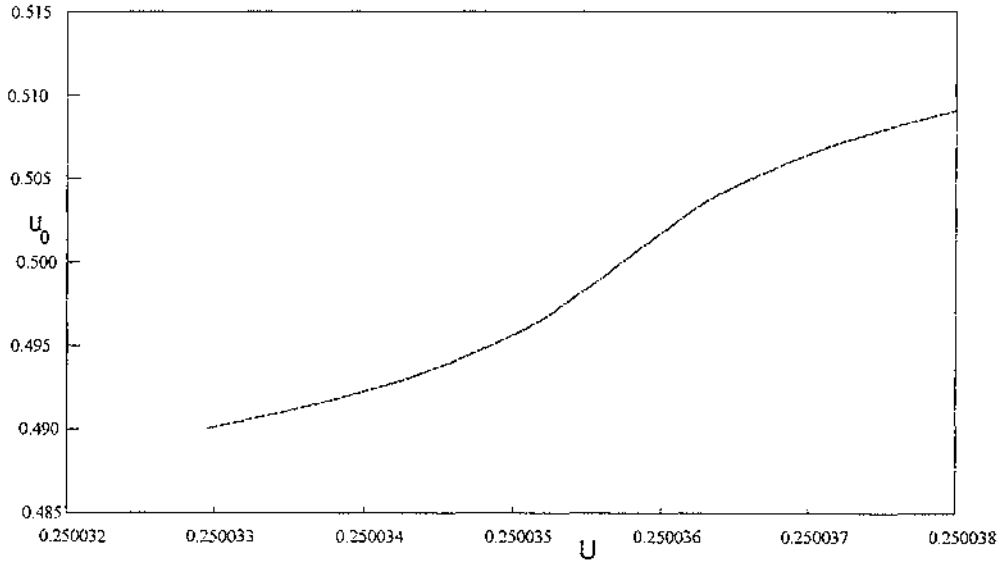

FIGURE 4.10 A view of the critical region in the u_0 versus U curve for $\lambda = 3.694$, using the approximation of u by u_{max}, the maximum value of u.

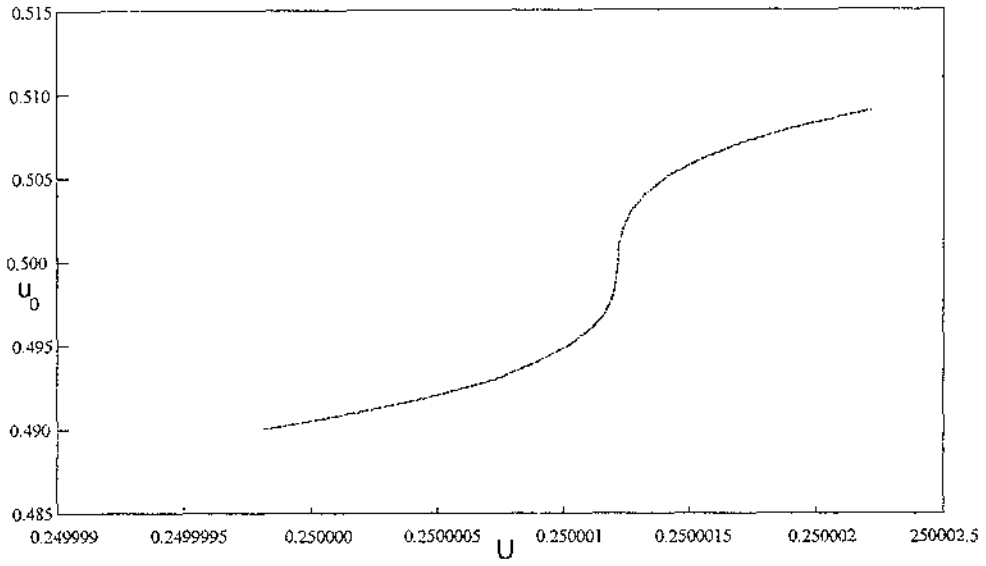

FIGURE 4.11 A view of the critical region in the u_0 versus U curve for $\lambda = 3.69451$, using the approximation of u by u_{max}, the maximum value of u.

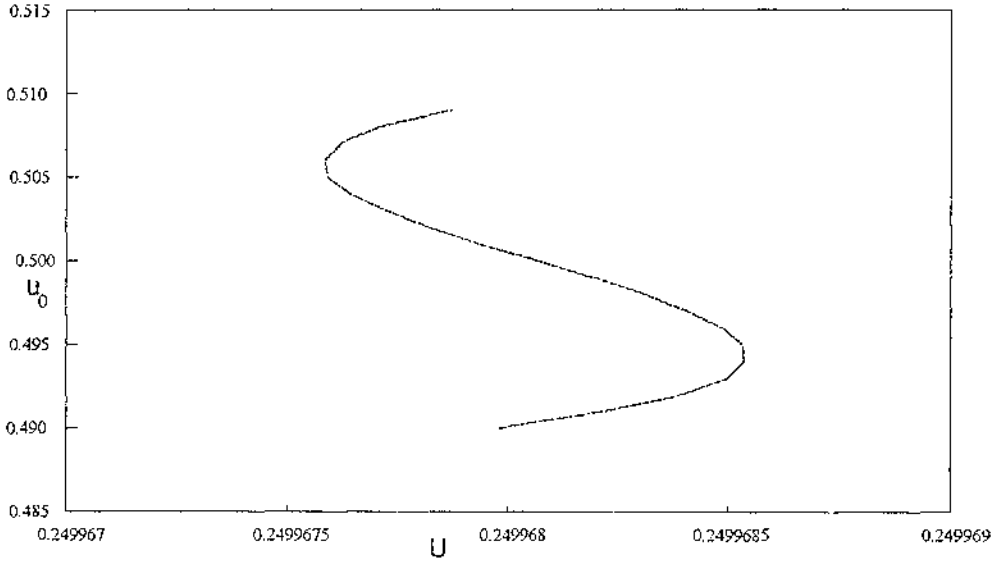

FIGURE 4.12 A view of the critical region in the u_0 versus U curve for $\lambda = 3.695$, using the approximation of u by u_{max}, the maximum value of u.

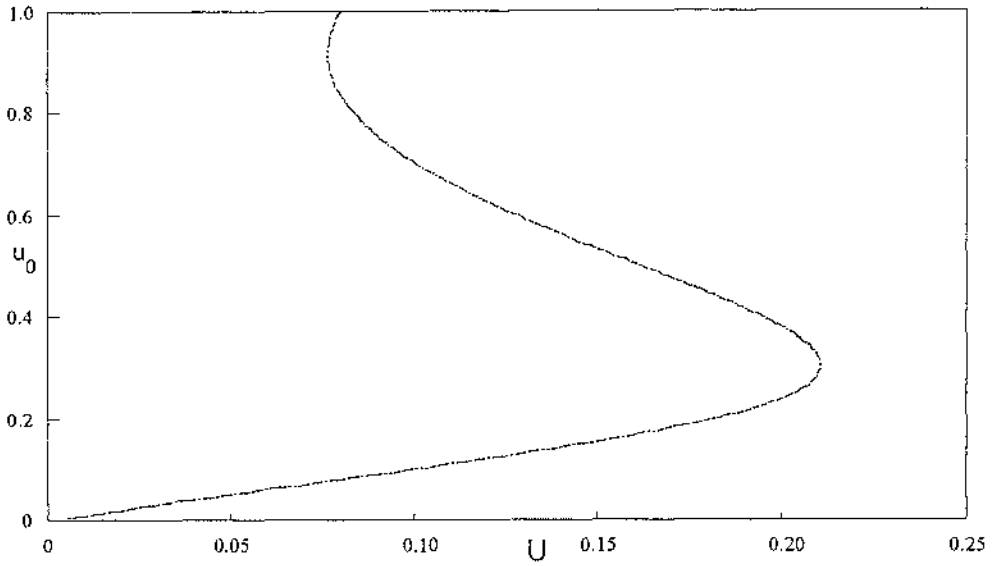

FIGURE 4.13 The u_0 versus U curve for $\lambda = 5$, using the approximation of u by u_{max}, the maximum value of u. The value of U_{cr} is 0.2108235.

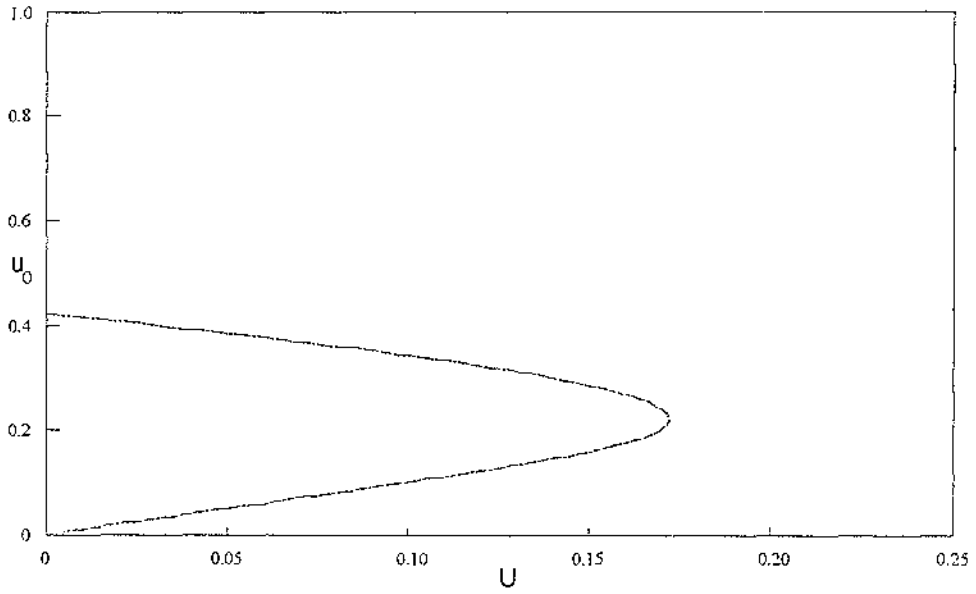

FIGURE 4.14 The u_0 versus U curve for $\lambda = 9$, using the approximation of u by u_{max}, the maximum value of u. The value of U_{cr} is 0.172238.

λ	U_{cr}	$u_{0,cr}$	λ	U_{cr}	$u_{0,cr}$
3.69451	0.250000	0.500	25	0.135934	0.162
3.70	0.249648	0.481	30	0.131317	0.1555
3.71	0.249040	0.469	35	0.127731	0.150
3.72	0.248459	0.461	40	0.124797	0.146
3.73	0.247898	0.454	45	0.122340	0.143
3.74	0.247352	0.4485	50	0.120238	0.140
3.75	0.246821	0.4435	55	0.118410	0.137
4	0.236074	0.3820	60	0.116798	0.135
5	0.210824	0.3025	65	0.115360	0.133
6	0.196117	0.268	70	0.114065	0.131
7	0.185935	0.247	75	0.112889	0.130
8	0.178283	0.2325	80	0.111816	0.128
9	0.172238	0.221	85	0.110829	0.127
10	0.167289	0.2125	90	0.109916	0.126
15	0.151315	0.186	95	0.109070	0.125
20	0.142146	0.172	100	0.108280	0.124

TABLE 4.2 Variation of U_{cr} and of $u_{0,cr}$ with λ for

$$\frac{d^2u}{dx^2} + \lambda \exp\left(-\frac{1}{u_{max}}\right) = 0, \quad -1 < x < 1$$

$$u(x) = u_a, \quad x = \pm 1$$

where U_{cr} is the largest value of U at which multiple solutions occur, $u_{0,cr}$ is the corresponding u_0 value, and u_{max} is the maximum value of $u(x)$. The number of significant figures reported represents the precision with which individual measurements were able to be made.

The maximum value of u(x) occurs at $x = 0$. From (7), when u_0 is small

$$u_a \cong u_0$$

so, substituting into (4.8),

$$\frac{du_a}{du_0} \approx 1$$

regardless of λ. For this reason, each curve has slope close to 1, for small values of U and u_0. U_{cr} appears to have a limiting value of 0.25, corresponding to a limiting $u_{0,cr}$ of 0.50.

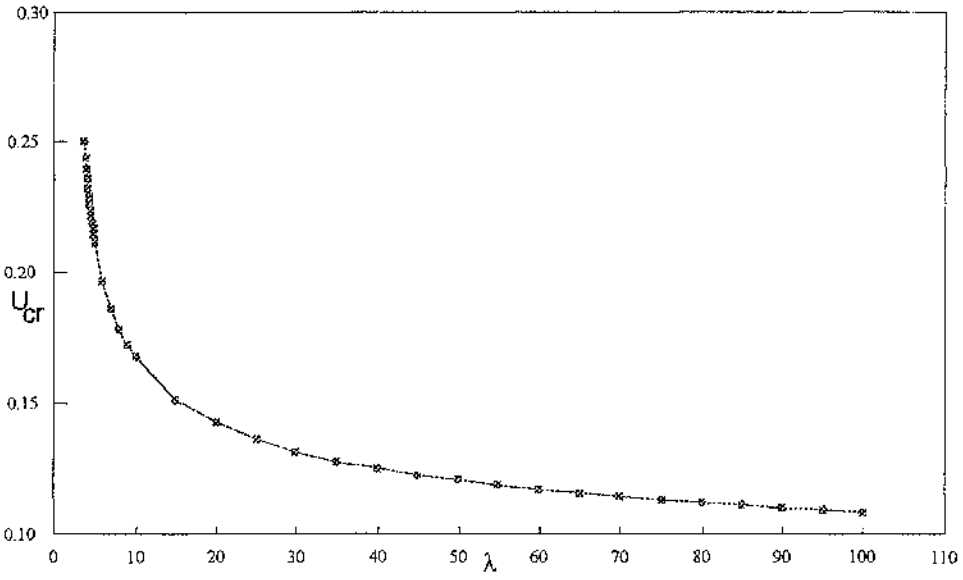

FIGURE 4.8 Variation of U_{cr} with λ for

$$\frac{d^2u}{dx^2} + \lambda \exp\left(-\frac{1}{u_{av}}\right) = 0, \quad -1 < x < 1,$$

$$u(x) = U, \quad x = \pm 1$$

where U_{cr} is the largest value of U at which multiple solutions occur, and u_{av} is the average value of $u(x)$. Data for this curve are contained in Table 4.1. Values of U_{cr} appear to approach a limit of 0.25; the minimum value of λ is 5.542517.

4.4 Approximation by relaxation

4.4.1 Relaxation method

The relaxation process attempts to solve equations of the form

$$\mathrm{Af} = \mathrm{b}$$

by iteratively examining the residuals which are the components of the vector

$$\mathrm{r}^{(k)} = \mathrm{b} - \mathrm{Af}^{(k)}$$

for the current solution $\mathrm{f}^{(k)}$. Successive changes are made in the components of $\mathrm{f}^{(k)}$ so that the components of the residual vector are reduced to negligible amounts.

4.4.2 Calculation of critical values

Rearranging (4.2),

$$u''(x) = -\lambda \exp\left(-\frac{1}{u}\right), \qquad u'(0) = 0,\ u(1) = U.$$

Also,

$$u''(x_n) = \frac{u(x_n - h) - 2u(x_n) + u(x_n + h)}{h^2}$$

where h is the step size and the index $n = 1,2,\ldots,1/\mathrm{h}$.

So

$$u_{n-1} - 2u_n + u_{n+1} = -\lambda h^2 \exp\left(-\frac{1}{u_n}\right).$$

where $u_m = u(x_m)$.

Since $u'(0) = 0$,

$$u_{-1} = u_1.$$

Then

$$u_0'' = \frac{u_{-1} - 2u_0 + u_1}{h^2}$$

$$= \frac{2}{h^2}(u_1 - u_0).$$

So

$$
\begin{aligned}
-2u_0 \quad +2u_1 \qquad\qquad\qquad\qquad\qquad\qquad &= -\lambda h^2 \exp\left(-\frac{1}{u_0}\right) \\
u_0 \quad -2u_1 \quad +u_2 \qquad\qquad\qquad\qquad &= -\lambda h^2 \exp\left(-\frac{1}{u_1}\right) \\
\qquad\qquad\qquad \ddots \qquad\qquad\qquad\qquad &\vdots \\
\qquad\qquad\qquad\qquad u_{n-3} \quad -2u_{n-2} \quad +u_{n-1} \qquad &= -\lambda h^2 \exp\left(-\frac{1}{u_{n-2}}\right) \\
\qquad\qquad\qquad\qquad\qquad\qquad u_{n-2} \quad -2u_{n-1} \quad +u_n \quad &= -\lambda h^2 \exp\left(-\frac{1}{u_{n-1}}\right)
\end{aligned}
$$

and $u_n = U$.

In matrix form and rearranging,

$$
\begin{pmatrix}
-2 & 2 & & & & & \\
1 & -2 & 1 & & & \mathrm{O} & \\
 & 1 & -2 & 1 & & & \\
 & & & \ddots & & & \\
 & \mathrm{O} & & & 1 & -2 & 1 \\
 & & & & & 1 & -2
\end{pmatrix}
\begin{pmatrix} u_0 \\ u_1 \\ u_2 \\ \vdots \\ u_{n-2} \\ u_{n-1} \end{pmatrix}
+ \lambda h^2
\begin{pmatrix}
\exp\left(-\frac{1}{u_0}\right) \\
\exp\left(-\frac{1}{u_0}\right) \\
\exp\left(-\frac{1}{u_0}\right) \\
\vdots \\
\exp\left(-\frac{1}{u_{n-2}}\right) \\
\exp\left(-\frac{1}{u_{n-1}}\right)
\end{pmatrix}
+
\begin{pmatrix} 0 \\ 0 \\ 0 \\ \vdots \\ 0 \\ U \end{pmatrix}
= \underline{\mathrm{O}}
$$

which is of the form $\underline{F}(\underline{u}) = \underline{0}$.

Then

$$\underline{u}^{(k+1)} = \underline{u} - J^{-1}\left(\underline{u}^{(k)}\right)\underline{F}\left(\underline{u}^{(k)}\right)$$

where the Jacobean

$$J = A + \lambda h^2 \operatorname{diag}\left(-\frac{1}{u_0^2}\exp\left(-\frac{1}{u_0}\right), \ldots, -\frac{1}{u_{n-1}^2}\exp\left(-\frac{1}{u_{n-1}}\right)\right)$$

and A is the tridiagonal matrix.

The values of $u^{(k)}$ are progressively used to improve the value of $u^{(k+1)}$ until there is negligible difference between successive values of $u^{(k)}$ and $u^{(k+1)}$. At that point, the value of u_n can then be accepted as a valid U for the given values of u_0 and λ.

4.4.3 Results

Typical curves of u_0 versus U are shown in Figures 4.16 - 4.21. Because the U values are calculated from the u_0 values, there is an artificial jump discontinuity which appears at U_{cr}. The value of U_{cr} is thus easily determined by identifying the jump in values of u_0 for very small changes in U. For values of λ less than the λ_{tr} value of 4.618, the expected curve is visible and has the same form as the curves derived by the earlier approximation methods. Table 4.4 contains critical values of U and u_0 for specific values of λ. This data is plotted in Figure 4.22. The λ_{tr} value of 4.61836 occurred for $U_{c\,r}$= 0.245781 and $u_{0,c\,r}$= 0.541.

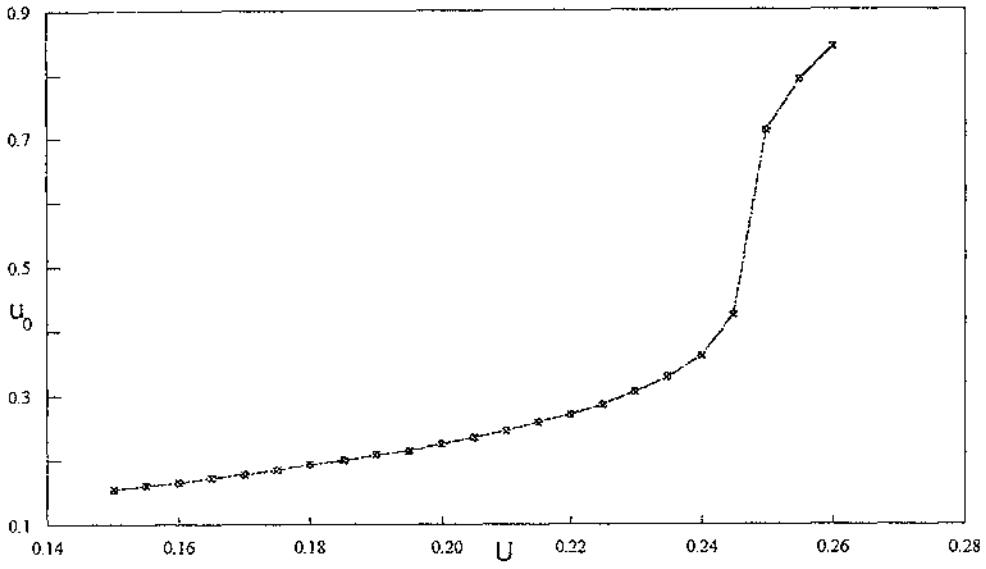

FIGURE 4.16 The u_0 versus U curve for $\lambda = 4.6$, calculated by numerical computation using the method of relaxation.

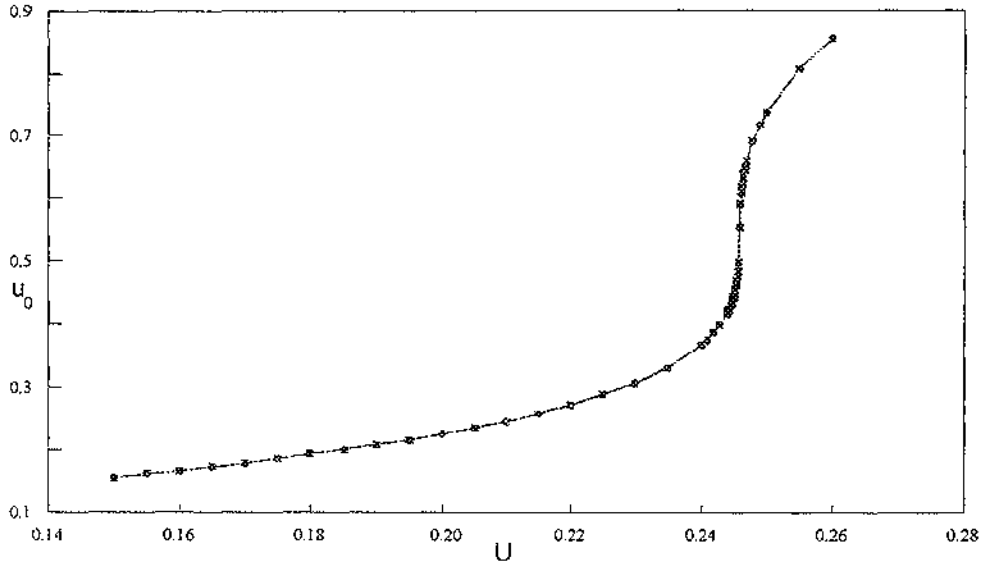

FIGURE 4.17 The u_0 versus U curve for $\lambda = 4.618$, calculated by numerical computation using the method of relaxation.

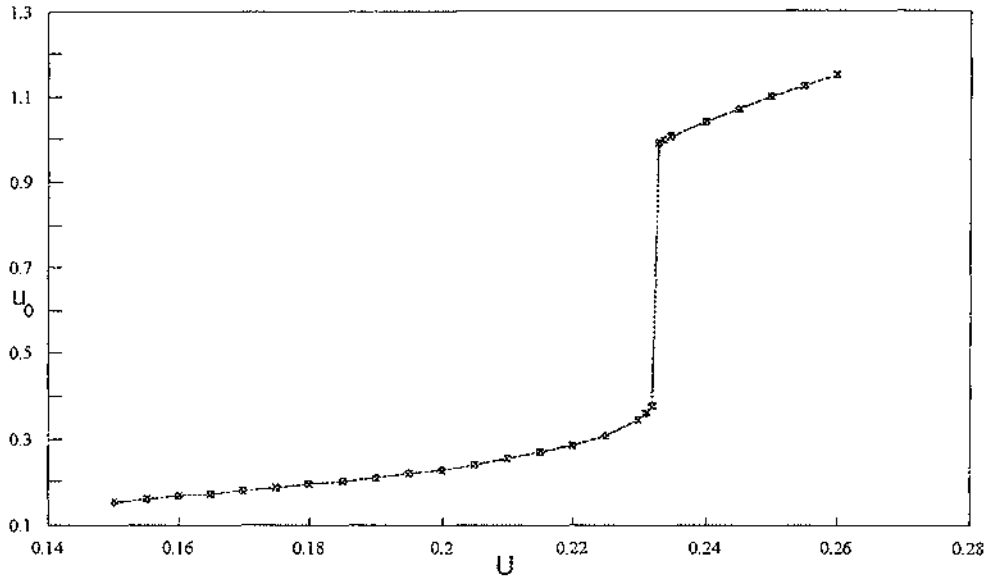

FIGURE 4.18 The u_0 versus U curve for $\lambda = 5$, calculated by numerical computation using the method of relaxation.

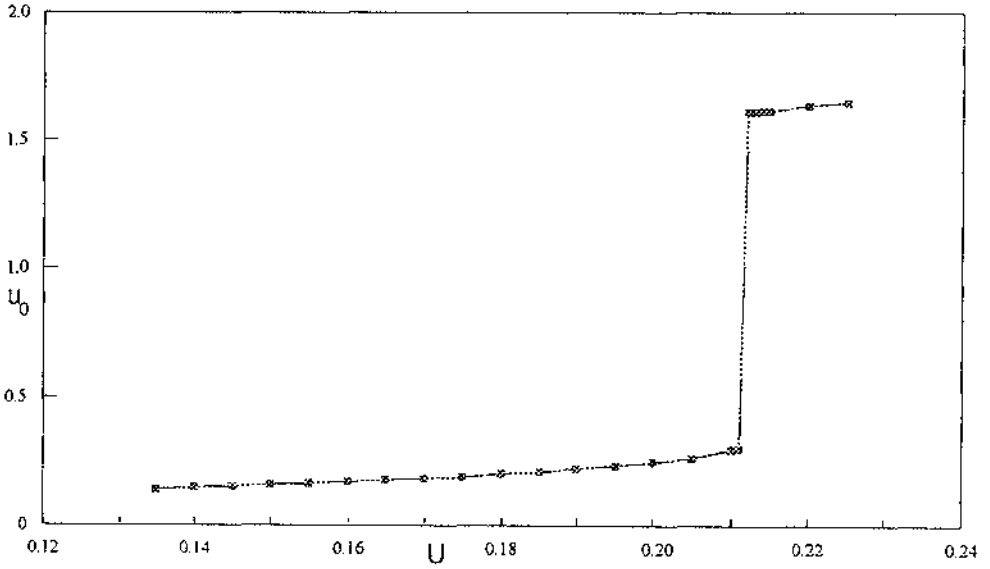

FIGURE 4.19 The u_0 versus U curve for $\lambda = 6$, calculated by numerical computation using the method of relaxation.

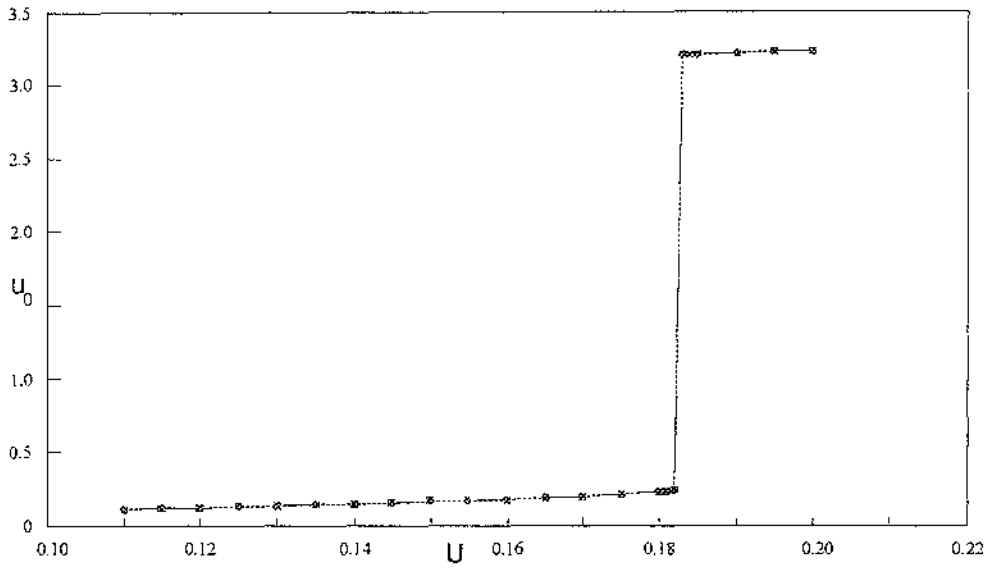

FIGURE 4.20 The u_0 versus U curve for $\lambda = 9$, calculated by numerical computation using the method of relaxation.

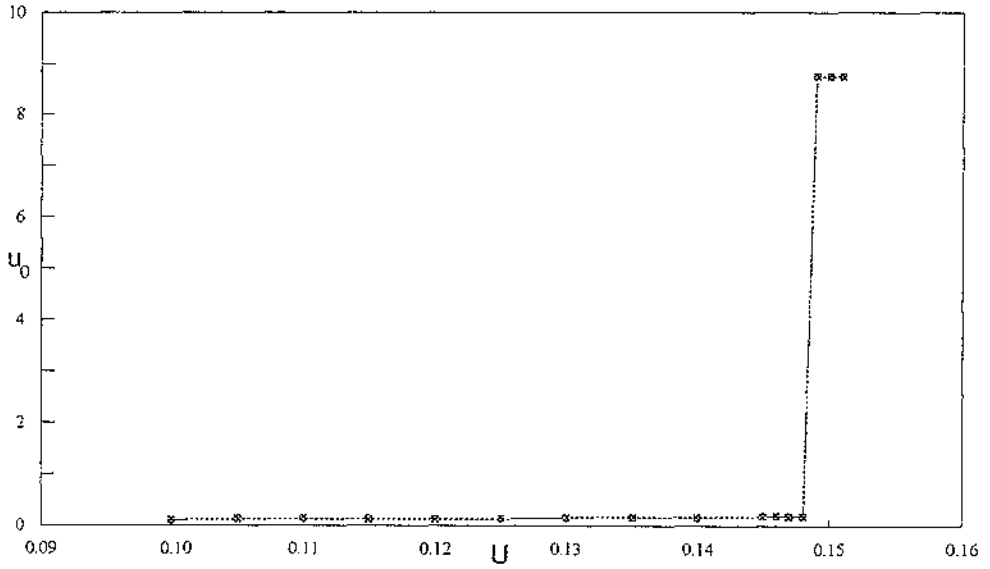

FIGURE 4.21 The u_0 versus U curve for $\lambda = 20$, calculated by numerical computation using the method of relaxation.

λ	U_{cr}	$u_{0,cr}$	λ	U_{cr}	$u_{0,cr}$
4.61836	0.245781	0.541	30	0.136017	0.168
4.62	0.245699	0.531	35	0.132089	0.162
4.65	0.244329	0.496	40	0.128904	0.157
4.70	0.242277	0.471	45	0.126246	0.153
4.80	0.238643	0.441	50	0.123977	0.149
4.90	0.235421	0.421	55	0.122008	0.146
5	0.232495	0.405	60	0.120276	0.144
6	0.211865	0.327	65	0.118731	0.142
7	0.198878	0.291	70	0.117343	0.139
8	0.189514	0.269	75	0.116087	0.138
9	0.182292	0.253	80	0.114941	0.136
10	0.176478	0.240	85	0.113884	0.135
15	0.158171	0.205	90	0.112913	0.133
20	0.147918	0.187	95	0.112011	0.132
25	0.141059	0.176	100	0.111168	0.131

TABLE 4.3 Variation of U_{cr} and $u_{0,cr}$ with λ when (4.2) is approximated by a numerical computation based on the method of relaxation.

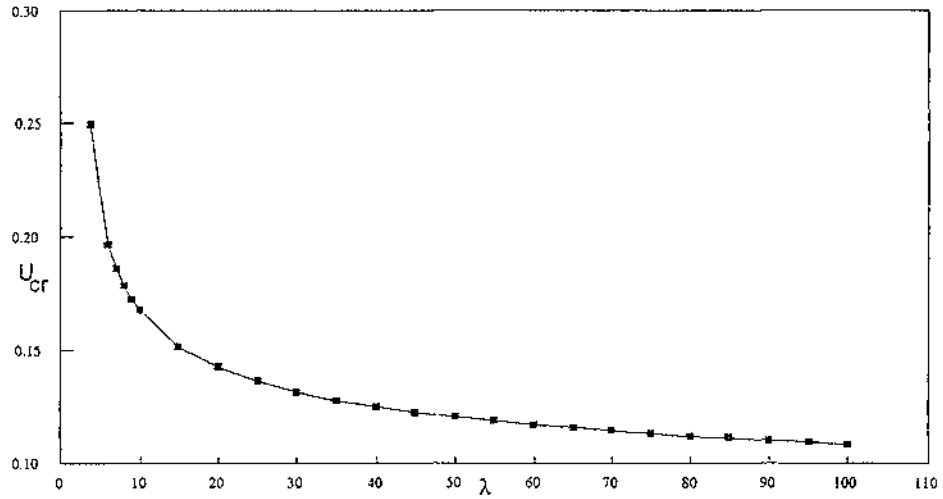

FIGURE 4.22 Variation of U_{cr} with λ. The data are contained in Table 4.3.

4.5 Comparison of results

Table 4.1 shows the U_{cr} values for various λ values. These are shown in Figure 4.23. At low U values, the curves are identical or at least very similar, with du_a/du_0 typically of value 1.

λ	U_{cr} values for approximation by average	maximum	relaxation
3.7		0.249648	
4.618			0.2458
5.542517	0.249967		
6	0.236073	0.196117	0.211865
7	0.217480	0.185935	0.198878
8	0.205205	0.178283	0.189514
9	0.196116	0.172238	0.182292
10	0.188979	0.167289	0.176478
15	0.167289	0.151315	0.158171
20	0.155528	0.142146	0.147918
25	0.147784	0.135934	0.141059
30	0.142142	0.131334	0.136017
35	0.137782	0.127731	0.132089
40	0.134253	0.124797	0.128904
45	0.131330	0.122340	0.126246
50	0.128832	0.120238	0.123977
55	0.126678	0.118410	0.122008
60	0.124796	0.116798	0.120276
65	0.123104	0.115360	0.118731
70	0.121597	0.114065	0.117343
75	0.120228	0.112889	0.116087
80	0.118993	0.111816	0.114941
85	0.117847	0.110829	0.113884
90	0.116798	0.109916	0.112913
95	0.115811	0.109070	0.112011
100	0.114909	0.108280	0.111168

TABLE 4.4 Comparison of methods.

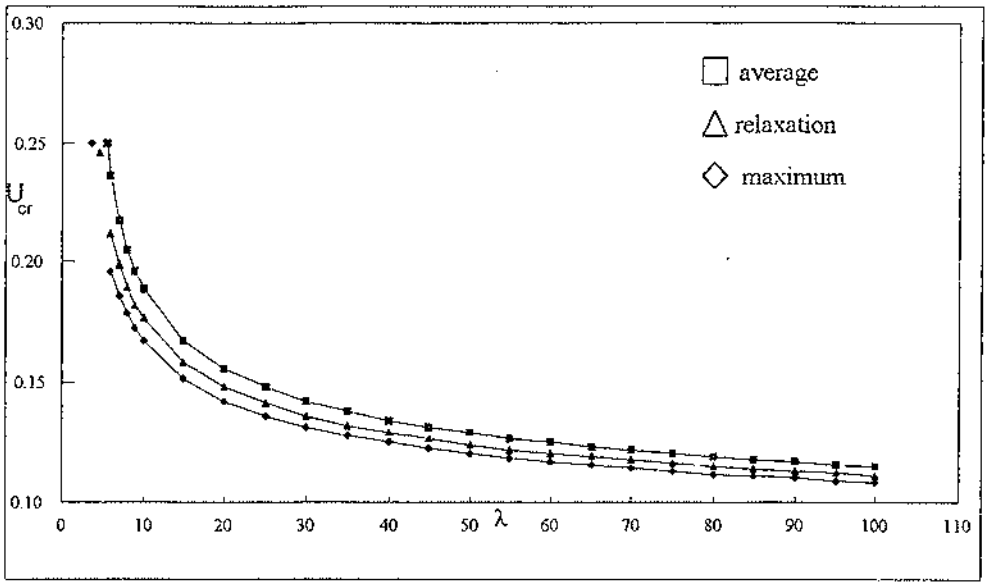

FIGURE 4.23 Comparison of methods.

The curve shown in Figure 4.23 can be extended to $\lambda = 1x10^{51}$. Such a curve has the same shape as that in the figure. The approximation by average yields consistently higher values for U_{cr} than either other method; the approximation by maximum consistently yields lower values for U_{cr} than either other method. A plot of $u_{0,cr}$ has the same form as that in Figure 4.23.

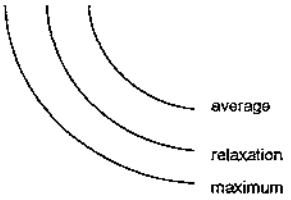

FIGURE 4.24

The approximations by average and by maximum yield u_{tr} values of 0.249967 and 0.250000, respectively. The approximation by relaxation yields a u_{tr} value of 0.245781, which compares well with the published value of 0.2459 [14].

More recently published values of U_{cr} [8] fall within the envelope created by the average and the maximum approximations, as shown in Figure 4.25. The λ_{tr} value of 4.618 is the same as that from the approximation by relaxation.

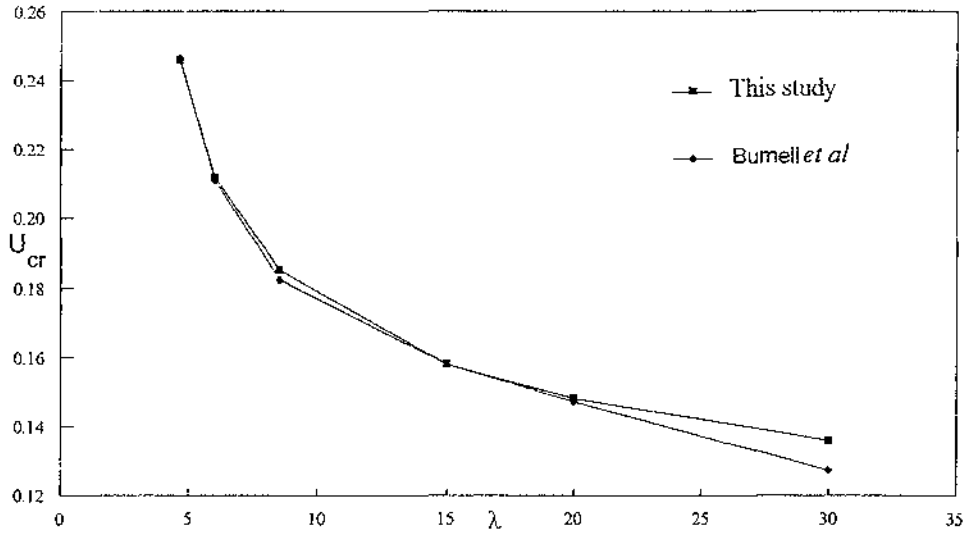

FIGURE 4.25 Comparison of results obtained by the method of relaxation in this study and the method used by Burnell [8].

Because all the curves have value $(U, u_0) = (0,0)$ and have slope = 1 for small values of both U and u_0, the initial part of the lower branch is almost identical regardless of method of approximation. This can be seen in Figure 4.26.

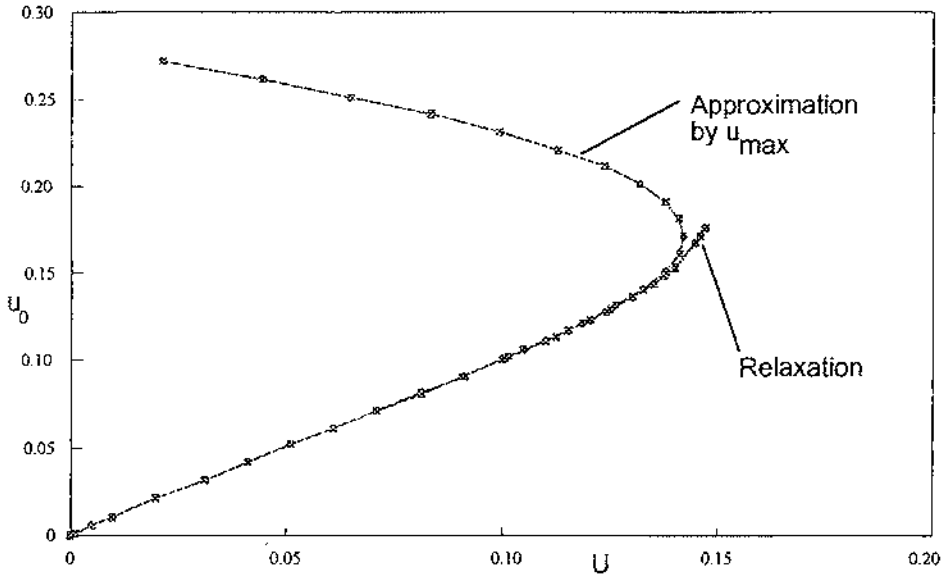

FIGURE 4.26 Superposition of curves created for λ = 20 using approximation by relaxation and approximation by u_{max}. The early part of each curve has slope = 1. At low U values, the curves are identical.

4.6 The upper branch

Once the lower branch impacts with $U = 0$, increasing values of u_0 result in negative values of U. Since these correspond to negative values of the absolute temperature, they are meaningless in a physical sense but interesting mathematically because eventually the values become less negative and ultimately the curve "re-emerges" into positive values for U. The aim of this section is to find a relationship between λ and the u_0 value at which this re-emergence takes place.

The methods of approximation by average u and by maximum u are unable to be used here because they would require the value of u_0 to be calculated at $U = 0$.The numerical computation method of relaxation, on the other hand, calculates only those values required by the step size, h. The step size can, therefore, be adjusted so that $U = 0$ is "stepped over" and not actually calculated.

Clearly, the sensitivity of the procedure is reduced by taking larger steps. Increased sensitivity is attained by keeping the step size small and only increasing it to avoid the value $U = 0$. The increase in step size should then be as small as necessary and should last just long enough for the purpose.

The curve for $\lambda = 8$ is shown in Figure 4.27. The value of $u_{0,cr}$ is 0.26861 and U_{cr} is 0.18951. The curve first strikes the u_0 axis at $u_0 = 0.7459$ and re-emerges at $u_0 = 2.2260$. The minimum U recorded was $U = -0.13817$ at $u_0 = 1.43144$.

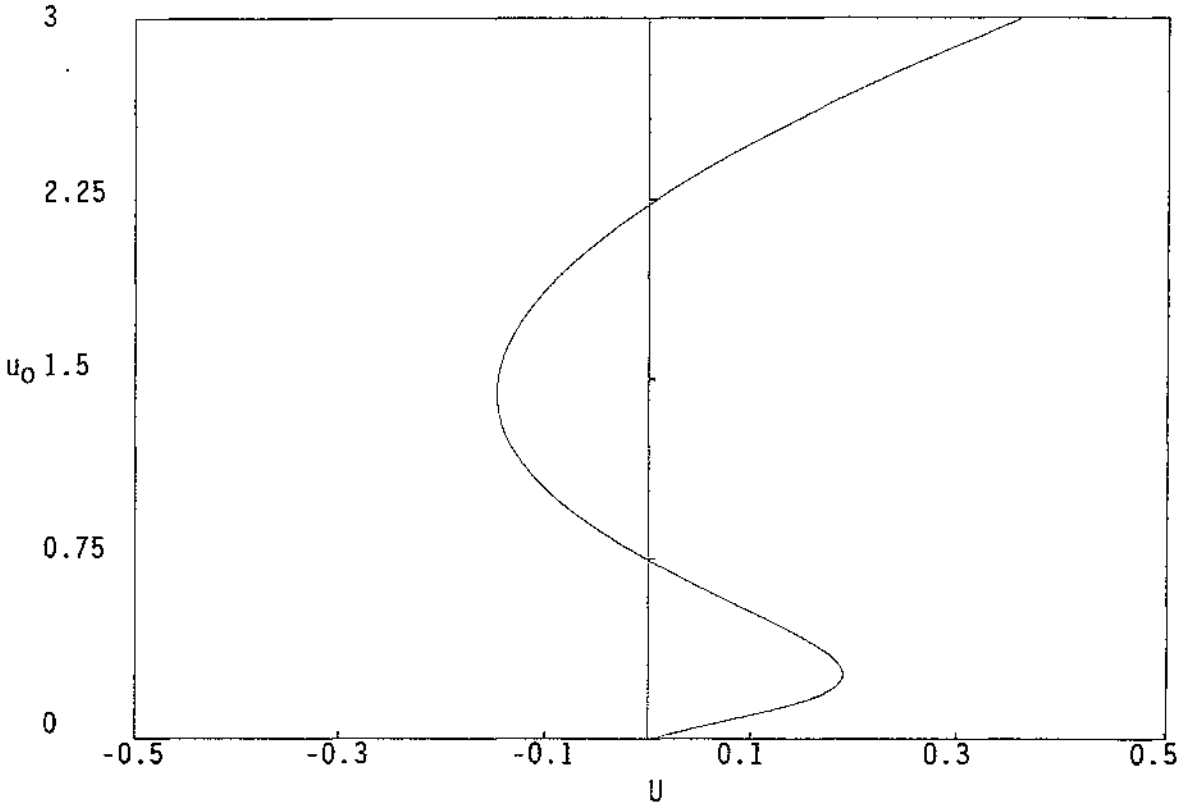

FIGURE 4.27 Bifurcation diagram for $\lambda = 8$.

For large values of λ, such as $\lambda = 1x10^{12}$, the upper arm is more difficult to find by computer because it involves very large numbers. A bisection method speeds up the search for the re-emergence point:

the first intersection with the u_0 axis is stored as a lower bound;
the value $u_0 = \lambda$ is an initial upper bound;
bisection progressively replaces the upper or lower bound until $U = 0$;
the corresponding u_0 is the point of re-emergence of the curve.

Results are shown in Table 4.5. The upper branch appears to start at about λ/2. In each case, the upper branch had slope = 1, for small values of U. This is to be expected for the same reasons as those which give the lower branch a slope of 1 for small values of U.

λ	U=0 lower branch	U=0 upper branch	U=0 upper branch (6 sig. fig.)
8	0.7459	1.43144	2.2260
$2.4x10^6$	1199998.6	0.06615	$1.20000x10^6$
$6x10^6$	2999998.5	0.06232	$3.00000x10^6$
$1x10^{12}$	4999999987367.6	0.03550	$5.00000x10^{11}$

TABLE 4.5 Identification of the upper branch.

4.7 Summary

The heat balance equation for combustion in the slab geometry, (4.2), can be approximated via the exponential term by replacing u by the average value of u and by the maximum value of u. In each case, the transition value, u_{tr} occurs at $u_{0,tr} = 0.25$ and $U_{tr} = 0.5$.

Equation (4.2) can also be approximated by a numerical computation method based on relaxation. This yields curves within an envelope bounded by the average approximation and by the maximum approximation.

All curves have slope = 1 for small values of U, regardless of λ, for the lower branch and for the upper branch.

The upper branch tends to include the point $(U, u_0) = (0, \lambda/2)$ as λ becomes large.

5 Spontaneous Ignition of Moist Milk Powder

5.1 Introduction

Fire in spray dryers for milk powder production can lead to dangerous situations for the operators, and may cause serious damage to plants and buildings. Dust explosion is usually the worst consequence of a fire [16].

It is known [2] [3] that spontaneous ignition of milk powder layers deposited on drying equipment is one of the causes of fire in dairy factories. See Figures 5.1 - 5.3. The situations that produce such a fire hazard must be defined quantitatively in order to set standards for effective preventative measures.

Several researchers, eg Beever [2], Duane [10] [11] and O'Mahoney [18], have studied in Europe the ignition characteristics of spray-dried milk powders of very low moisture contents, typically of 3%.

Extrapolation of the experimental conditions (usually at temperatures of greater than 120°C) to a practical situation involves an assumption that there is uniform heating at both sides of the slab in a layer geometry. In an industrial situation, however, often one side of the slab is hot whilst the other is not. For example, the wall temperature and the chamber temperature of a spray dryer are different once a layer of milk powder has built up. This has been taken into account in the current study.

Another aspect of the problem, which has not been explored so far, is the effect of drying on the powder ignition characteristics. The milk powder deposited on the drying chamber may include a considerable amount of moisture. After deposition has occurred the powder may undergo drying of its residual moisture, thus dissipating the heat generated by oxidation or other exothermic reactions, eg Maillard reactions. The hazard potential may thus be reduced. The critical level of moisture content beyond which the ignition hazard is minimised has been determined in the current study.

FIGURE 5.1 The result of a fire in a milk powder factory. Te Rapa, NZ, 1993.

FIGURE 5.2 Another view of the damaged milk powder plant. The heavy metal doors were lifted from their rollers and flung outside by the explosive blast. The door on the right is clearly at least two metres from the building.

FIGURE 5.3 Close-up view of the damaged milk powder plant. The roof has been destroyed, partly by the explosion, partly by the fire.

5.2 Mathematical model

5.2.1 The spontaneous ignition of dry powder

The spontaneous ignition of dry milk powder in the slab geometry has been predicted [12] by means of the steady-state non-linear heat conduction equation, which can be written in terms of

$$u = \frac{RT}{E} \quad \text{and} \quad U_i = \frac{RT_{a,i}}{E}, \quad i = 0,1$$

as

$$\frac{d^2u}{dx^2} + \lambda \exp\left(-\frac{1}{u}\right) = 0, \quad 0 < x < 1$$

$$u = U_0 \quad \text{at } x = 0$$

$$u = U_1 \quad \text{at } x = 1$$

where

$$\lambda = \frac{\sigma Q A R \ell_0^2}{kE}.$$

Here T is the absolute temperature, σ is the density, Q is the exothermicity, A is the frequency factor, R is the universal gas constant, k is the thermal conductivity, E the activation energy, and ℓ_0 is the thickness of the layer.

For this type of problem, the critical thickness, $\ell = \ell_{cr}$, is the parameter of interest for given values of all other constants and U_0 and U_1.

The bifurcation diagram [14] is shown in Figure 5.4. There is always a unique solution for small ℓ. For large values of U, the solution is unique for any ℓ. If ℓ is sufficiently large then multiple solutions exist for small values of U.

The value of ℓ at which the lower branch is discontinuous in λ is ℓ_{cr}. For $\ell > \ell_{cr}$ the system is able to migrate to the upper branch, resulting in thermal ignition. Identification of this fold bifurcation point thus identifies the onset of thermal ignition.

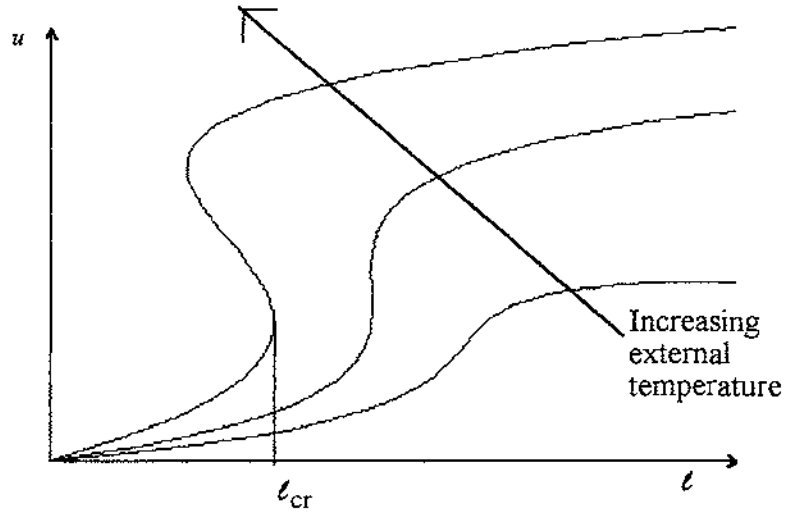

FIGURE 5.4. Bifurcation diagram for the ignition of dry powder. The thickness of powder, ℓ, has a critical value, ℓ_{cr}, at which thermal ignition will occur. At this value, the system migrates to the higher energy branch.

5.2.2 The spontaneous ignition of moist powder

In order to react, molecules must reach a certain critical energy, E, known as the activation energy. The rate constant for such a reaction is

$$k^* = A\exp\left(-\frac{E}{RT}\right)$$

where A is the frequency factor. The fraction of molecules with the energy necessary to react is $\exp(-E/RT)$ which can be written as $\exp(-1/u)$, where

$$u = \frac{RT}{E}.$$

Then

$$\lambda \propto \frac{Q}{k}.$$

During the vaporisation of water,

$$H_2O_{(\ell)} \rightarrow H_2O_{(g)},$$

heat which is added to the system is absorbed as the latent heat of vaporisation, ΔH_V. This absorbed energy does not raise the temperature of the water; instead, it converts the water from the liquid state to the higher energy gaseous state.

Assuming that the reaction is not reversible and that no equilibrium is reached, the change in entropy

$$\Delta S_v = S_{(\ell)} - S_{(g)} = \frac{\Delta H_v}{T_b}$$

is equal to the ratio of latent heat of vaporisation to that of boiling point of water.

Over the temperature range of this study, 90°C to 190°C, the latent heat of vaporisation of water varies by about 13%.

Moisture in a wet powder may be trapped in interstitial spaces or it may be bound to the solid. Drying is the process of removing both the trapped moisture and the bound moisture. Thus, the heat of drying is the sum of the latent heat of vaporisation of water plus the work required to drive off the bound moisture.

In this study, the heat of drying varies with temperature and with water content, as given by [12]

Heat of drying = Latent heat of vaporisation + Work to drive off bound moisture

$$= \left(2502371.493 - 2498.841629\left(T - 273.15\right)\right) + \frac{RT\left(\frac{W_p}{0.047}\right)^{-\frac{1}{0.787}}}{0.018} \text{ J kg}^{-1}.$$

For simplicity and without loss of generality, the value T can be taken as the average of the wall temperature and chamber temperature, each measured as the absolute temperature.

During combustion of moist milk powder, heat is generated by the dry reaction and removed by the heat of drying.

Neglecting any chemical reaction between water and milk powder and assuming no condensation of water vapour, the spontaneous ignition of moist milk powder in the slab geometry and in the steady-state formulation can be written as

$$\frac{d^2u}{dx^2}+\lambda\left(\exp\left(-\frac{1}{u}\right)-\beta\exp\left(-\frac{\alpha}{u}\right)\right)=0,\quad 0<x<1 \qquad (5.1)$$

$$u(0)=u_0$$

$$u(1)=U$$

where

$$\alpha=\frac{\Delta H_v}{E}$$

$$\beta=\frac{\Delta H_v A_1}{QA}$$

$$\lambda=\frac{\rho R\ell^2 QA}{k_w E}$$

$$u=\frac{RT}{E}$$

and the parameter α represents the ratio of latent heat to that of activation energy. The dimensionless parameter β is proportional to water content which is expressed as a percentage, W_p.

$$\lambda \propto \frac{\text{thickness}^2 \times \text{ exothermicity of the dry reaction}}{\text{thermal conductivity}}.$$

The frequency factor for the vaporisation of water is A_1; Q is the exothermicity; ℓ is the height of milk powder.

The exothermicity, Q, is a measure of the difference between the energy of the reactant molecules and the energy of the product molecules in a reaction. In an exothermic reaction, energy is released.

The thermal conductivity of moist powder, k_W, is calculated [22] from

$$\frac{1}{k_w}=0.75\left(\frac{1}{(1-\varphi)\lambda_s+\varphi\lambda_a}\right)+0.25\left(\frac{1-\varphi}{\lambda_s}+\frac{\varphi}{\lambda_a}\right)$$

where the proportion of the packing density due to water is

$$\varphi = 1 - \frac{\text{density of milk powder}}{\text{packing density}}$$
$$= 1 - \frac{\rho}{\rho_{pw}},$$

with empirical relationships

$$\lambda_s = 0.132\left(1 + 0.0052\left(T - 273.15\right)\right)$$
$$\lambda_a = \frac{1005\mu_a}{\text{Pr}}$$
$$\mu_a = \frac{1.097 \times 10^{-6}\sqrt{T}}{1.453 - 0.0243\sqrt{T}}$$
$$\text{Pr} = 0.71 - 0.00015\left(T - 273.15\right)$$

and typical values shown in Table 5.1.

T (°C)	λ_s (x 10^{-1})	λ_a (x 10^{-2})	μ_a (x 10^{-5})	Pr (x 10^{-1})
90	1.93776	3.0471	2.1118	6.9650
100	2.00640	3.1154	2.1544	6.9500
110	2.07504	3.1839	2.1971	6.9350
120	2.14368	3.2527	2.2397	6.9200
130	2.21232	3.3218	2.2823	6.9050
140	2.28096	3.3912	2.3249	6.8900
150	2.34960	3.4609	2.3676	6.8750
160	2.41824	3.5310	2.4102	6.8600
170	2.48688	3.6014	2.4529	6.8450
180	2.55552	3.6722	2.4956	6.8300
190	2.62416	3.7434	2.5384	6.8150

TABLE 5.1 Empirical values.

The overall density is

$$\rho_{pw} = \frac{\rho_{dry} + w_p \rho_{water}}{1 + w_p}$$

where the density of water is

$$\rho_{water} = 1000 \exp\left(-\left[0.0182 + 0.0018(T - 273.15)\right]^2\right)$$

and ρ_{dry} is the density of the dry powder.

Heat generated by the dry reaction is represented by λ exp (-1/u); heat removed by drying is represented by $\lambda\beta$ exp ($-\alpha$/u). The bifurcation diagram is shown in Figure 5.5.

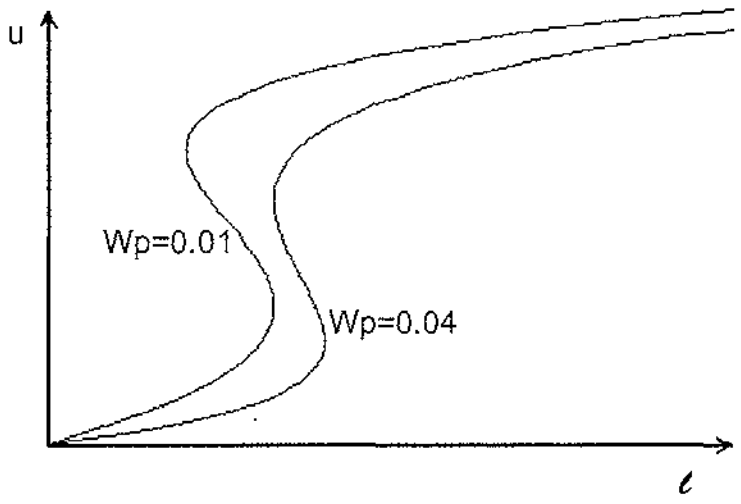

FIGURE 5.5 The bifurcation diagram for the combustion of moist milk powder. As the water content, w_p, increases, the fold bifurcation point occurs at higher values of thickness, ℓ.

5.3 Software Implementation

The software package AUTO [9], which performs bifurcation analysis on dynamical systems, was applied to the combustion of moist milk powder. The two point boundary value problem (5.1) is reduced to a system of differential equations.

Since the exponential terms are too small for effective computation, a scaling factor, F, is included. The system becomes

$$u_1' = u_2$$

$$u_2' = -\lambda\left(\exp\left(-\frac{1}{u_1}+F\right)-\beta\exp\left(-\frac{\alpha}{u_1}+F\right)\right)$$

$$u_1(x=0) = u_0 = \frac{RT_0}{E}$$

$$u_1(x=1) = u_1 = \frac{RT_1}{E}$$

$$F = \ln\frac{\lambda}{\lambda^*}$$

where T_e and T_1 represent the chamber and wall temperatures respectively.

Since AUTO requires an initial starting solution, λ=0 is chosen without complication. AUTO returns the value λ^*.

The required value ℓ is then determined from

$$\ell = \sqrt{\frac{\lambda^* \exp(F) k_w E}{\rho R Q A}}.$$

The fold bifurcation point determines the critical size of the pile of moist powder. As the water content, W_p, increases, the value of β increases and the fold bifurcation point disappears.

5.4 Results

Typical results, for moisture levels 1%, 2%, 3% and 4%, are shown in Table 5.3. These results are shown graphically in Figures 5.6 to 5.9.

1%	90	100	110	120	130	140	150	160	170	180	190
90	0.1586										
100	0.1270	0.1043									
110	0.1004	0.0844	0.0702								
120	0.0791	0.0680	0.0577	0.0483							
130	0.0620	0.0543	0.0469	0.0401	0.0339						
140	0.0485	0.0432	0.0380	0.0330	0.0284	0.0242					
150	0.0381	0.0343	0.0306	0.0271	0.0245	0.0210	0.0176				
160	0.0300	0.0273	0.0247	0.0221	0.0196	0.0172	0.0150	0.0130			
170	0.0238	0.0218	0.0199	0.0180	0.0162	0.0144	0.0128	0.0112	0.0097		
180	0.0189	0.0175	0.0161	0.0147	0.0134	0.0120	0.0108	0.0096	0.0084	0.0074	
190	0.0151	0.0141	0.0131	0.0120	0.0110	0.0100	0.0091	0.0082	0.0073	0.0065	0.0057

2%	90	100	110	120	130	140	150	160	170	180	190
90	-										
100	-	-									
110	0.1723	0.1219	0.0936								
120	0.1075	0.0882	0.0731	0.0574							
130	0.0760	0.0651	0.0551	0.0459	0.0379						
140	0.0559	0.0492	0.0428	0.0367	0.0311	0.0262					
150	0.0422	0.0378	0.0335	0.0294	0.0255	0.0223	0.0186				
160	0.0323	0.0294	0.0264	0.0236	0.0208	0.0182	0.0157	0.0135			
170	0.0251	0.0230	0.0210	0.0189	0.0170	0.0151	0.0133	0.0116	0.0097		
180	0.0197	0.0182	0.0168	0.0153	0.0139	0.0125	0.0111	0.0099	0.0087	0.0076	
190	0.0156	0.0146	0.0135	0.0124	0.0114	0.0103	0.0093	0.0084	0.0074	0.0066	0.0058

3%	90	100	110	120	130	140	150	160	170	180	190
90	-										
100	-	-									
110	-	-	-								
120	-	-	-	-							
130	-	-	-	-	-						
140	-	-	-	-	-	-					
150	-	-	-	-	0.0461	0.0341	0.0246				
160	0.0508	0.0453	0.0394	0.0330	0.0282	0.0235	0.0194	0.0160			
170	0.0323	0.0295	0.0266	0.0237	0.0208	0.0180	0.0155	0.0133	0.0113		
180	0.0233	0.0215	0.0197	0.0179	0.0160	0.0143	0.0126	0.0110	0.0095	0.0082	
190	0.0176	0.0164	0.0151	0.0139	0.0127	0.0114	0.0103	0.0091	0.0080	0.0071	0.0062

4%	90	100	110	120	130	140	150	160	170	180	190
90	-										
10	-	-									
110	-	-	-								
120	-	-	-	-							
130	-	-	-	-	-						
140	-	-	-	-	-	-					
150	-	-	-	-	-	-	-				
160	-	-	-	-	-	-	-	-			
170	-	-	-	-	-	-	-	-	0.0156		
180	-	-	-	-	-	0.0241	0.0183	0.0146	0.0119	0.0097	
190	0.0231	0.0216	0.0200	0.0183	0.0164	0.0146	0.0127	0.0110	0.0094	0.0081	0.0069

TABLE 5.2. Critical height in metres for combinations of wall and chamber temperatures at different moisture content levels.

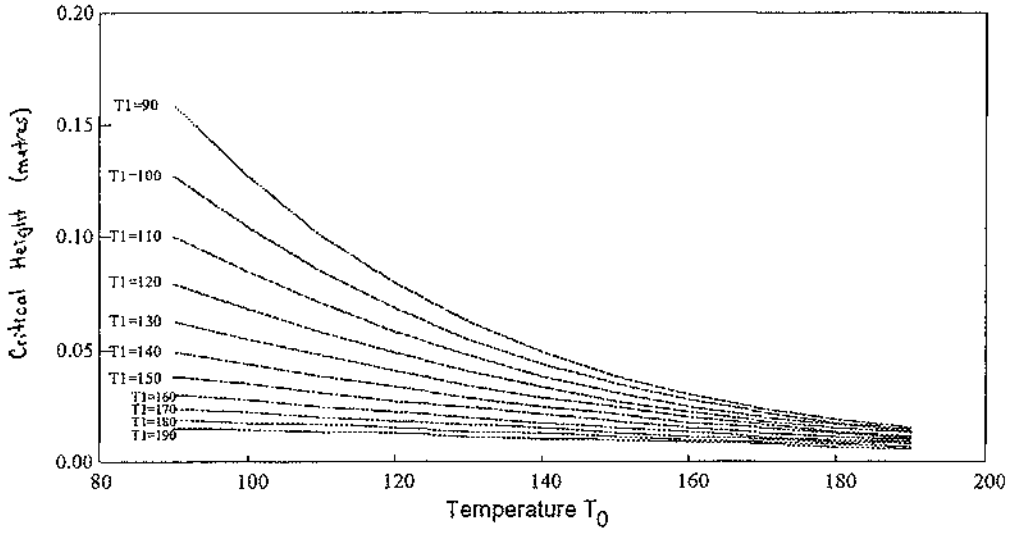

FIGURE 5.6 Critical heights for various temperature combinations for whole milk powder containing 1% moisture.

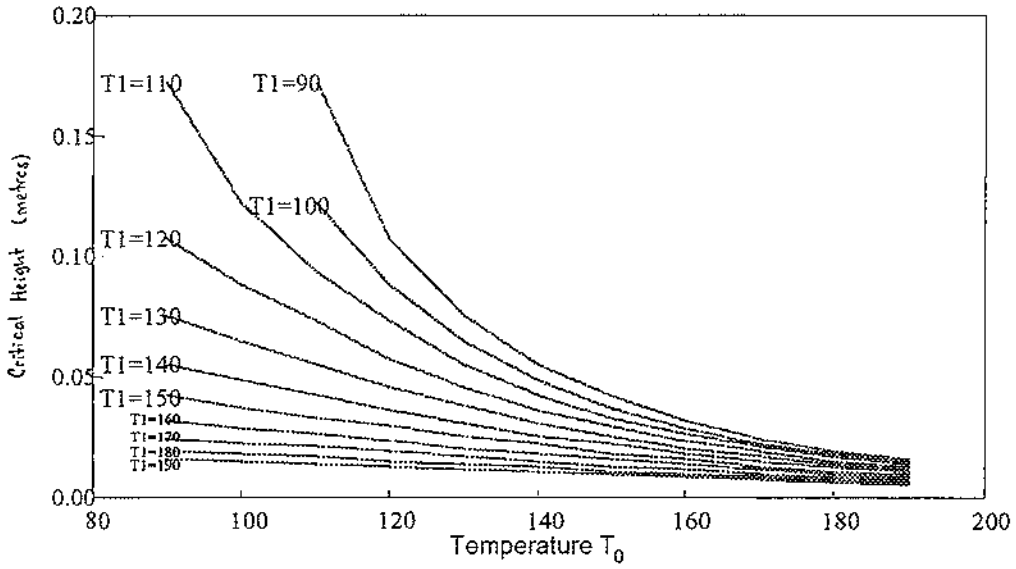

FIGURE 5.7 Critical heights for various temperature combinations for whole milk powder containing 2% moisture.

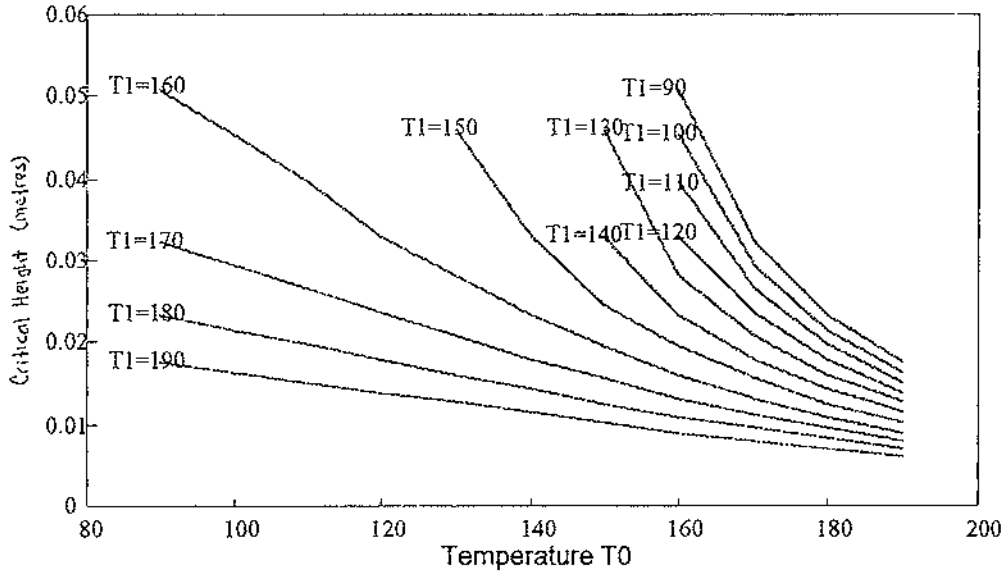

FIGURE 5.8 Critical heights for various temperature combinations for whole milk powder containing 3% moisture.

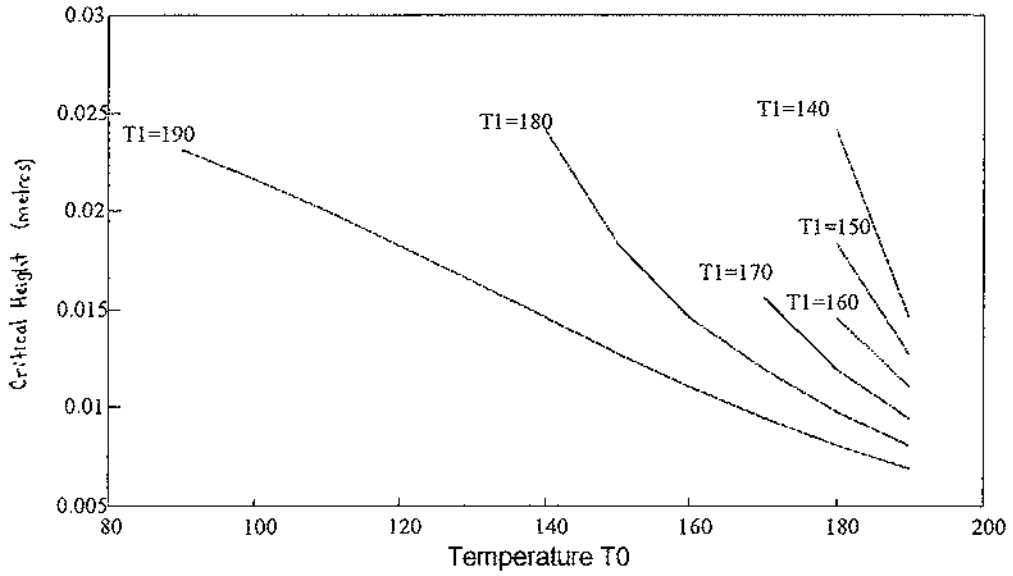

FIGURE 5.9 Critical heights for various temperature combinations for whole milk powder containing 4% moisture.

5.5 Comparison with Frank-Kamenetskii Variables

Using the old Frank-Kamenetskii variables, (5.1) can be written as

$$\frac{d^2\theta}{dx^2} + \delta \exp\theta = 0, \quad 0 < x < 1,$$
$$\theta(0) = \theta_0, \quad \theta(1) = \theta_1$$

where

$$\theta = \frac{E}{RT^2}\left(T - T_a\right)$$
$$T_a = \frac{T_0 + T_1}{2}$$
$$\delta \propto \frac{\text{thickness}^2 \times \text{exothermicity}}{\text{thermal conductivity}}.$$

Under this formulation, it has been shown [12] that the critical heights for dry milk powder are those given in Table 5.4, below. Using the same data but with the Gray Wake variables used elsewhere in this study, the critical heights for dry milk powder can be calculated as above. These heights are shown in Table 5.3.

	90	100	110	120	130	140	150	160	170	180	190
90	0.1765										
100	0.1489	0.1258									
110	0.1233	0.1066	0.0914								
120	0.1018	0.0894	0.0778	0.0672							
130	0.0838	0.0746	0.0659	0.0577	0.0503						
140	0.0690	0.0622	0.0556	0.0493	0.0435	0.0387					
150	0.0569	0.0518	0.0468	0.0420	0.0375	0.0333	0.0293				
160	0.0470	0.0432	0.0394	0.0361	0.0322	0.0289	0.0258	0.0229			
170	0.0390	0.0361	0.0332	0.0304	0.0277	0.0251	0.0226	0.0202	0.0180		
180	0.0325	0.0303	0.0281	0.0259	0.0238	0.0217	0.0197	0.0178	0.0160	0.0144	
190	0.0272	0.0255	0.0238	0.0221	0.0204	0.0188	0.0172	0.0157	0.0142	0.0129	0.0116

TABLE 5.3 Critical height, in metres, for combinations of wall and chamber temperatures using the Gray Wake variables.

	90	100	110	120	130	140	150	160	170	180	190
90	0.1545										
100	0.1319	0.1139									
110	0.1116	0.0973	0.0839								
120	0.0934	0.0822	0.0717	0.0619							
130	0.0773	0.0687	0.0605	0.0527	0.0454						
140	0.0636	0.0570	0.0506	0.0446	0.0388	0.0334					
150	0.0519	0.0468	0.0420	0.0373	0.0328	0.0286	0.0247				
160	0.0418	0.0381	0.0344	0.0309	0.0274	0.0241	0.0210	0.0181			
170	0.0337	0.0308	0.0281	0.0254	0.0227	0.0202	0.0178	0.0154	0.0133		
180	0.0269	0.0248	0.0227	0.0207	0.0187	0.0167	0.0149	0.0131	0.0114	0.0098	
190	0.0214	0.0199	0.0183	0.0168	0.0152	0.0138	0.0123	0.0109	0.0096	0.0084	0.0072

TABLE 5.4. Critical height, in metres, for combinations of wall and chamber temperatures using the Frank-Kamenetskii variables.

	90	100	110	120	130	140	150	160	170	180	190
90	0.0220										
100	0.0170	0.0119									
110	0.0117	0.0093	0.0075								
120	0.0084	0.0072	0.0061	0.0053							
130	0.0065	0.0059	0.0054	0.0050	0.0049						
140	0.0054	0.0052	0.0050	0.0047	0.0047	0.0053					
150	0.0050	0.0050	0.0048	0.0047	0.0047	0.0047	0.0046				
160	0.0052	0.0051	0.0050	0.0052	0.0048	0.0048	0.0048	0.0048			
170	0.0053	0.0053	0.0051	0.0050	0.0050	0.0049	0.0048	0.0048	0.0047		
180	0.0056	0.0055	0.0054	0.0052	0.0051	0.0050	0.0048	0.0047	0.0046	0.0046	
190	0.0058	0.0056	0.0055	0.0053	0.0052	0.0050	0.0049	0.0048	0.0046	0.0045	0.0044

TABLE 5.5 Actual differences between values in Tables 5.3 and 5.4.

	90	100	110	120	130	140	150	160	170	180	190
90	12.5										
100	11.4	9.4									
110	9.5	8.8	8.2								
120	8.2	8.0	7.9	7.9							
130	7.8	7.9	8.2	8.7	9.7						
140	7.8	8.3	9.0	9.6	10.8	13.6					
150	8.8	9.6	10.3	11.3	12.6	14.2	15.8				
160	11.1	11.8	12.7	14.5	15.0	16.6	18.5	20.8			
170	13.6	14.7	15.4	16.5	18.0	19.4	21.1	23.8	26.3		
180	17.2	18.1	19.1	20.0	21.3	23.0	24.4	26.5	28.9	31.9	
190	21.3	21.8	23.0	23.9	25.5	26.5	28.5	30.5	32.5	34.7	37.9

TABLE 5.6 Percentage differences between values in Tables 5.3 and 5.4.

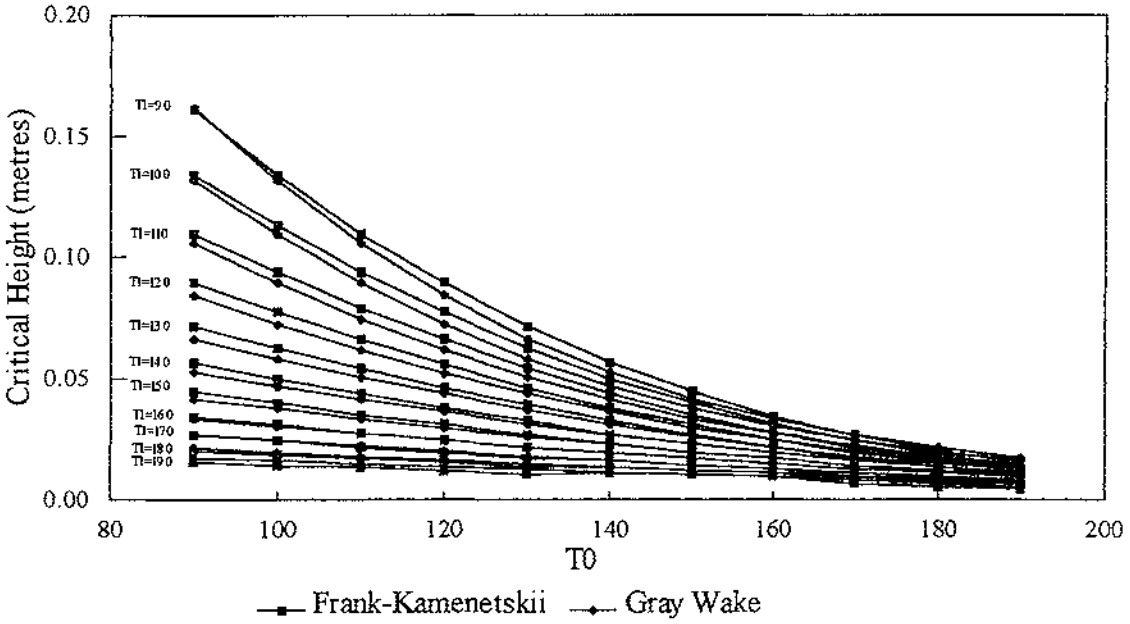

FIGURE 5.10 Critical height, in metres, of dry milk powder, for combinations of wall and chamber temperatures using the Frank-Kamenetskii and Gray Wake variables.

REFERENCES

[1] Balakrishnan, E., Swift, A. and Wake, G.C. Path-following for disjoint bifurcation problems arising in ignition theory. *In press.*

[2] Beever, P. Spontaneous ignition of milk powders in a spray-drying plant. *Journal of the Society of Dairy Technology* **37** (2), (1984) 68-71.

[3] Beever, P. and Crowhurst, D. Fire and explosion hazards associated with milk spray drying operations. *Journal of the Society of Dairy Technology* **42** (3), (1989) 65-70.

[4] Boddington, T., Gray, P., Harvey, D.I. Thermal theory of spontaneous ignition: criticality in bodies of arbitrary shape. *Philosophical Transactions of the Royal Society* **A270** (1971), 467 - 506.

[5] Boddington, T., Gray, P., Wake, G.C. Criteria for thermal explosions with and without reactant consumption. *Proceedings of the Royal Society of London* **A357** (1977), 403 - 422.

[6] Bowes, P.C. A general approach to the prediction and control of potential runaway reaction. *Runaway reactions, Unstable Products and Combustible Powders,* IChemE Symposium Series No.68, (1981).

[7] Burnell, J.G., Graham-Eagle, J.G., Gray, B.F., Wake, G.C. A new scaling of a problem in combustion theory. *Reaction-Diffusion Equations*, Oxford Science, (1990), 25 - 38.

[8] Burnell, J.G., Graham-Eagle, J.G., Gray, B.F., Wake, G.C. Determination of critical ambient temperatures for thermal ignition. *IMA Journal of Applied Mathematics* (1989) **42**, 149 - 153.

[9] Doedel, E. *AUTO: software for continuation and bifurcation problems in ordinary differential equations*, California Institute of Technology, U.S.A., (1986).

[10] Duane, T.C. and Synott, E.C. Effect of some physical properties of milk powders on mimimum ignition temperature. *I. Chem. E. Symposium Series* No.68. (1981) 2/J:1-8.

[11] Duane, T.C. and Synott, E.C. Ignition characteristics of spray-dried milk product powders in oven tests. *Journal of Food Engineering* **17** (1992) 163-176.

[12] Dairy Research Institute of New Zealand. *Private communication.*

[13] Frank-Kamenetskii, D.A. *Diffusion and heat transfer in chemical kinetics.* University Press, Princeton, NJ edition, (1955).

[14] Gray, B.F. and Wake G.C. On the determination of critical ambient temperatures and critical ignition temperatures for thermal ignition. *Combustion and Flame* **71** (1988) 101 - 104.

[15] Gray, B.F., Merkin J.H., Wake G.C. Disjoint Bifurcation diagrams in combustion systems. *Mathl Comput. Modelling* **15** No.11 (1991) 25 - 33.

[16] International Dairy Federation *Bulletin of the International Dairy Federation*, No.219 (1987).

[17] Lacey, A.A. and Wake, G.C. Critical initial conditions for spatially-distributed thermal explosions. *J. Austral. Math. Soc. Ser. B* **33** (1992), 350 - 362.

[18] O'Mahoney, J.G. and Synott, Z.C. Influence of sample shape and size on self-ignition of a fat-filled milk powder. *Journal of Food Engineering* **7** (1988) 271 - 280.

[19] Parks, J.R. Criticality criteria for various configurations of a self-heating chemical as functions of activation energy and temperature of assembly.

[20] Sisson, R.A., Swift, A., Wake, G.C. Spontaneous ignition of materials on hot surfaces. *Mathematical Engineering in Industry* **2** No.4 (1990), 287 - 301.

[21] Rogers, G.F.C. and Mayhew, Y.R., *Thermodynamic and Transport Properties of Fluids*.

[22] Sano, Y. and Keey, R.B. The drying of a spherical particle containing colloidal material into a hollow sphere. *Chemical Engineering Science* **37** (1982) No.6, 881-889.